nature reviews methods primers

https://doi.org/10.1038/s43586-023-00243-w

Primer

Check for updates

Photocatalytic CO_2 reduction

Siyuan Fang[1], Motiar Rahaman[2], Jaya Bharti[3], Erwin Reisner[2], Marc Robert[3,4], Geoffrey A. Ozin[5] & Yun Hang Hu[1]

Abstract

Using sunlight to power CO_2 conversion into value-added chemicals and fuels is a promising technology to use anthropogenic CO_2 emissions for alleviating our dependence on fossil fuels. In this Primer, we provide a holistic step-by-step guide for the experimentation of photocatalytic CO_2 reduction, including catalyst synthesis and characterization, reactor construction, photocatalytic testing and mechanism exploration. We compare and analyse the state-of-the-art results with different photocatalysts and discuss possible reaction mechanisms. Furthermore, important considerations regarding practical application of photocatalytic CO_2 reduction are highlighted and strategies to enhance energy conversion efficiency and product selectivity are summarized. This Primer also reveals current issues of reproducibility, standardizes data reporting and proposes a unified operation condition. Finally, future directions are outlined in terms of experiments, calculations, big-data development and practical application.

Sections

[1]Department of Materials Science and Engineering, Michigan Technological University, Houghton, MI, USA. [2]Yusuf Hamied Department of Chemistry, University of Cambridge, Cambridge, UK. [3]Laboratoire d'Electrochimie Moléculaire, Université Paris Cité, CNRS, Paris, France. [4]Institut Universitaire de France, Paris, France. [5]Department of Chemistry, University of Toronto, Toronto, Ontario, Canada. e-mail: yunhangh@mtu.edu

Introduction

The content of carbon dioxide (CO_2) in the atmosphere has significantly increased to 420 ppm from approximately 280 ppm in the early 1800s[1,2]. This is mainly due to the extensive exploitation of fossil fuels, with the current global fossil CO_2 emissions having reached 36.3 gigatonnes per year and continuing to grow[2]. This linear fossil-to-CO_2 economy model is causing global warming, sea level rise, ocean acidification, extreme weather, species extinction and food shortage[3,4]. The development of efficient decarbonization technologies to capture, store and utilize CO_2 could mitigate these issues.

CO_2 capture and geological sequestration require large energy consumption, but the utilization of CO_2 as a feedstock for producing value-added chemicals and fuels is an attractive long-term proposition to complete the carbon cycle[5–9]. For example, CO_2 can be converted into carbon monoxide (CO), formic acid (HCOOH), formaldehyde (HCHO), methanol (CH_3OH), methane (CH_4) as well as multicarbon chemicals such as oxalic acid ($H_2C_2O_4$), acetic acid (CH_3COOH), acetaldehyde (CH_3CHO), ethanol (CH_3CH_2OH), ethylene (C_2H_4) and ethane (C_2H_6) via a series of reduction reactions. As summarized in Table 1, these products have high market prices, ranging from 0.1 US$ per kg to 2.0 US$ per kg, with broad applications in chemical production, clean fuels, metallurgy, solvation, disinfection, bleaching, food and beverage, the leather and textile industry and cryogenic refrigeration systems[10].

Many approaches have been explored for CO_2 conversion to date, including thermal catalysis, electrocatalysis and photocatalysis. Thermal catalysis generally shows high efficiencies for CO_2 reduction, but harsh conditions with high temperatures and high pressures are often required, causing considerable energy cost and safety issues[11,12]. Electrocatalysis is performed under an external electric field, in which there is a trade-off between the catalytic activity and selectivity, owing to the excessive overpotential[13,14]. By contrast, photocatalysis relies on solar energy for CO_2 reduction, demonstrating several advantages such as mild operation condition, small energy consumption and ready availability[15,16]. Therefore, photocatalytic CO_2 reduction has attracted enormous research interests since the pioneering work to drive CO_2 reduction into HCHO and CH_3OH[17] by illuminating the aqueous suspensions of various semiconductor powders including TiO_2, ZnO, CdS, GaP and SiC.

Photocatalytic CO_2 reduction approaches can be categorized into heterogeneous process and homogeneous process. Heterogeneous processes are typically based on semiconductor or plasmonic metal solid photocatalysts. As illustrated in Fig. 1a, photocatalytic CO_2 reduction over a semiconductor photocatalyst undergoes at least three mechanistic steps[5,18]. First, light with photon energy equal to or greater than the semiconductor energy band gap is absorbed, exciting the electrons from the valence band maximum (VBM) to the conduction band minimum (CBM), while leaving holes at the VBM. Next, the photo-generated electrons and holes transfer to the catalyst surface (through cocatalyst if applicable). Finally, adsorbed CO_2 is reduced by photo-generated electrons and the adsorbed reductant is oxidized by photo-generated holes. Ideally, CO_2 reduction is accompanied by water oxidation or some other value-added oxidations. Moreover, such a process must satisfy two thermodynamic requirements. Namely, the redox potential of reduction half-reaction must be more positive than the CBM, and the redox potential of oxidation half-reaction must be more negative than the VBM. Common CO_2 reduction half-reactions and the corresponding apparent standard redox potentials (at pH = 7) are summarized in Table 1. In addition, from the perspective of reaction kinetics, there must be catalytic sites in which CO_2 activation takes place.

It is effective to fabricate heterostructure catalysts with favourable band alignment to enable broad spectral responses and efficient charge separation. According to charge transfer directions, heterostructure catalysts are divided into p–n junction and *Z*-scheme[19–23]. In a p–n junction (Fig. 1b), photo-generated electrons are injected into the component with more positive CB position, whereas photo-generated holes migrate to the component with more negative VB position. Differently, in a Z-scheme architecture (Fig. 1c), photo-generated electrons in the component with more positive CB position are injected into the VB of another component with a more negative position either directly or indirectly with conductive intermediate or reversible redox shuttle.

Furthermore, heterogeneous photocatalytic CO_2 reduction can be carried out over metal catalysts such as gold, silver, copper and bismuth, which mainly owes to the localized surface plasmon resonance effect[24–27] (Fig. 1d). Namely, after collective oscillation of surface electrons is excited by incident photons at the resonant frequency, local heat is generated and hot charge carriers are formed through intraband *s*-to-*s* or interband *d*-to-*s* transitions under the strong surface electric field[28]. Both the local heat and hot charge carriers can contribute to CO_2 reduction[27,29].

The mechanistic steps of homogeneous photocatalytic CO_2 reduction are similar to those over semiconductor catalysts, although with the participation of photosensitizer and molecular catalyst instead. As shown in Fig. 1e, the photosensitizer is excited upon light absorption and then reductively quenched by the reductant, forming a reduced photosensitizer molecule[30]. The reduced photosensitizer injects electrons to the molecular catalyst, transforming it from the oxidized state to the reduced state. The reduced molecular catalyst then donates electrons to CO_2 to realize its reduction. The alternative mechanism of oxidative quenching is less common in photocatalytic CO_2 reduction processes[31]. Furthermore, there are hybrid processes in which a molecular catalyst is attached to a heterogeneous semiconductor via covalent or non-covalent interactions[32]. In this case, the semiconductor is responsible for charge carrier excitation, whereas the molecular catalyst provides active sites for CO_2 reduction (performing as a cocatalyst).

This Primer focuses on photocatalytic approaches to convert CO_2 into value-added chemicals and fuels. A general method for conducting photocatalytic CO_2 reduction experiments is summarized in terms of catalyst synthesis, catalyst characterization, experimental setup, photocatalytic test and mechanism exploration. Afterwards, a state-of-the-art overview on important metrics and possible mechanisms of photocatalytic CO_2 reduction is provided, followed by an in-depth analysis of the considerations for its practical application. This Primer also reveals the factors hindering reproducibility and elucidates the data reporting requirements and standard operation condition. Finally, the main limitations and corresponding optimization strategies are discussed, and future directions are outlined.

Experimentation

A general overview for conducting photocatalytic CO_2 reduction experiments is presented in Fig. 2, including five steps, namely, catalyst synthesis, catalyst characterization, assembly of the photocatalytic reactor, performing photocatalytic tests and exploring reaction mechanisms.

Catalyst synthesis

The photocatalytic system applied for CO_2 reduction generally consists of a light absorber and cocatalyst. In many cases, the light absorber and cocatalyst are synthesized independently and then combined to give

a functional assembly. In heterogeneous photocatalytic systems, light absorbers are mainly metals[24,25,33] and alloys[34], organic frameworks such as metal–organic frameworks (MOFs)[35–38] and covalent organic frameworks (COFs)[39–41] or inorganic semiconductors. Typical inorganic semiconductors include metal oxides[42–45], metal sulfides[39,46–48], metal oxyhalides[49–51], layered double hydroxides[34,52] and graphene-like 2D materials (such as g-C_3N_4 and graphene oxide)[21,50,53–59]. Most of the inorganic semiconductors are commercially available. However, inorganic semiconductors with various crystal phases, morphologies, particle sizes and defects (or vacancies) can be synthesized to provide more insights into the structure–property–performance relationship and acquire more flexibility to achieve the optimal photocatalytic performance. Synthesis methods of the inorganic semiconductors include calcination, hydrothermal or solvothermal reaction, co-precipitation, chemical vapour deposition, ultrasonication, laser ablation and mechanical exfoliation[15,50], whereas metals and alloys are generally prepared by reducing corresponding metal ions or metal oxides via chemical, electrochemical or photochemical approaches[24,25,33]. The synthesis of organic frameworks is more complicated because the reaction condition must allow the formation of well-defined building blocks while avoiding the decomposition of organic linkers[60]. Besides room-temperature synthesis routes, the electric heating, microwave, mechanochemistry, electrochemistry and ultrasonic techniques have also been exploited for preparing MOFs and COFs[60–62].

Distinctively, the light absorber in homogeneous photocatalytic systems represents the photosensitizer. Metal (such as ruthenium, iridium, platinum and copper) complex photosensitizers, which are prepared via a series of organic reactions, are the most widely used, owing to their various excited-state electronic configurations and long-lived triplet states[63–66]. In addition, organic photosensitizers (without any metals) have been developed and optimized via molecular engineering to attain the desirable solubility, stability and lifetime of excited states[65,67]. Furthermore, carbon nanodots, which possess tunable surface chemistry, low toxicity and scalable synthetic routes, are an alternative to those molecularly defined complexes[68]. Carbon nanodots are synthesized via either top-down approaches with the breakdown of graphite, graphene or soot, or bottom-up approaches by thermally decomposing cheap organic molecular precursors or polymers[68,69].

Cocatalysts. Cocatalysts can have a crucial role in heterogeneous photocatalytic CO_2 reduction processes[5,70,71]. First, they can improve the separation and migration of photo-generated electrons and holes and thus enhance the activity. This also enhances the robustness of the photocatalyst for long-term processes by efficiently consuming the photo-generated electrons (for CO_2 reduction) and holes (for the counter water or substrate oxidation). Furthermore, they can help to lower the activation energy or overpotential of CO_2 conversion process to improve the reaction kinetics and can direct the selectivity of CO_2 reduction towards a desired product and suppress parasitic side reactions, such as H_2 evolution reaction.

The major cocatalysts applied for heterogeneous photocatalytic CO_2 reduction include metals[42,72–74] and alloys[75,76]; metal compounds[5] such as metal oxides[77,78], metal hydroxides[79], metal sulfides[80], metal carbides[81] and metal nitrides[82]; graphene-based materials[54,83]; enzymes[84–89]; bacteria[90–92]; and metal complexes[20,48,57,93,94]. In addition, surface defects can be created as pseudo cocatalysts that serve as catalytically active sites[35,45,47,95,96]. Metal compound cocatalysts are synthesized via various approaches such as hydrothermal or solvothermal reactions[77,80] and high-temperature gas–solid reactions[82].

Table 1 | Common products of photocatalytic CO_2 reduction

Product	Half-reaction of CO_2 reduction	Redox potential (V)[a]	Annual production (10^9 kg)[b]	Market price (US$ per kg)[b]	Relevant uses[c]
CO	$CO_2+2e^-+2H^+\rightarrow CO+H_2O$	−0.52	32	0.1	Fischer–Tropsch synthesis, carbonylation of alkenes, metallurgy
$HCOO^-$	$CO_2+2e^-+H^+\rightarrow HCOO^-$	−0.41	0.7	0.9	Preservative and antibacterial agent in livestock feed, leather and textile industry
HCHO	$CO_2+4e^-+4H^+\rightarrow HCHO+H_2O$	−0.48	23	0.4	Production of resins and polyfunctional alcohols, disinfection
CH_3OH	$CO_2+6e^-+6H^+\rightarrow CH_3OH+H_2O$	−0.38	85	0.6	Gasoline additive, fuel, production of HCHO, CH_3COOH and methyl *tert*-butyl ether
CH_4	$CO_2+8e^-+8H^+\rightarrow CH_4+2H_2O$	−0.24	2,650	0.4	Fuel, reforming to syngas
$C_2O_4^{2-}$	$2CO_2+2e^-\rightarrow C_2O_4^{2-}$	−1.00	0.4	1.6	Cleaning, bleaching
CH_3COO^-	$2CO_2+8e^-+7H^+\rightarrow CH_3COO^-+2H_2O$	−0.29	12	1.4	Solvent, food, production of vinyl acetate, acetic anhydride and ester
CH_3CHO	$2CO_2+10e^-+10H^+\rightarrow CH_3CHO+3H_2O$	−0.36	1.0	2.0	Production of 2-ethyl-1-octanol and pentaerythritol
CH_3CH_2OH	$2CO_2+12e^-+12H^+\rightarrow CH_3CH_2OH+3H_2O$	−0.33	81	1.1	Fuel, solvent, alcoholic beverage, antiseptic in medical uses
C_2H_4	$2CO_2+12e^-+12H^+\rightarrow C_2H_4+4H_2O$	−0.35	214	1.2	Production of ethylene oxide, ethylene dichloride, ethylbenzene and polyethylene
C_2H_6	$2CO_2+14e^-+14H^+\rightarrow C_2H_6+4H_2O$	−0.27	134	0.2	Production of C_2H_4, power generation, cryogenic refrigeration system

[a]The values of apparent standard redox potentials are relative to standard hydrogen electrode (SHE) at pH=7 (refs. 5,209,210). [b]The annual productions and market prices in 2022 are mainly acquired from US Energy Information Administration and ChemAnalyst. [c]The relevant uses of CO_2 reduction products are referenced to ref. 10. The listed annual productions, market prices and relevant uses of $HCOO^-$, $C_2O_4^{2-}$ and CH_3COO^- represent those of their conjugate acids, namely, HCOOH, $H_2C_2O_4$ and CH_3COOH, respectively.

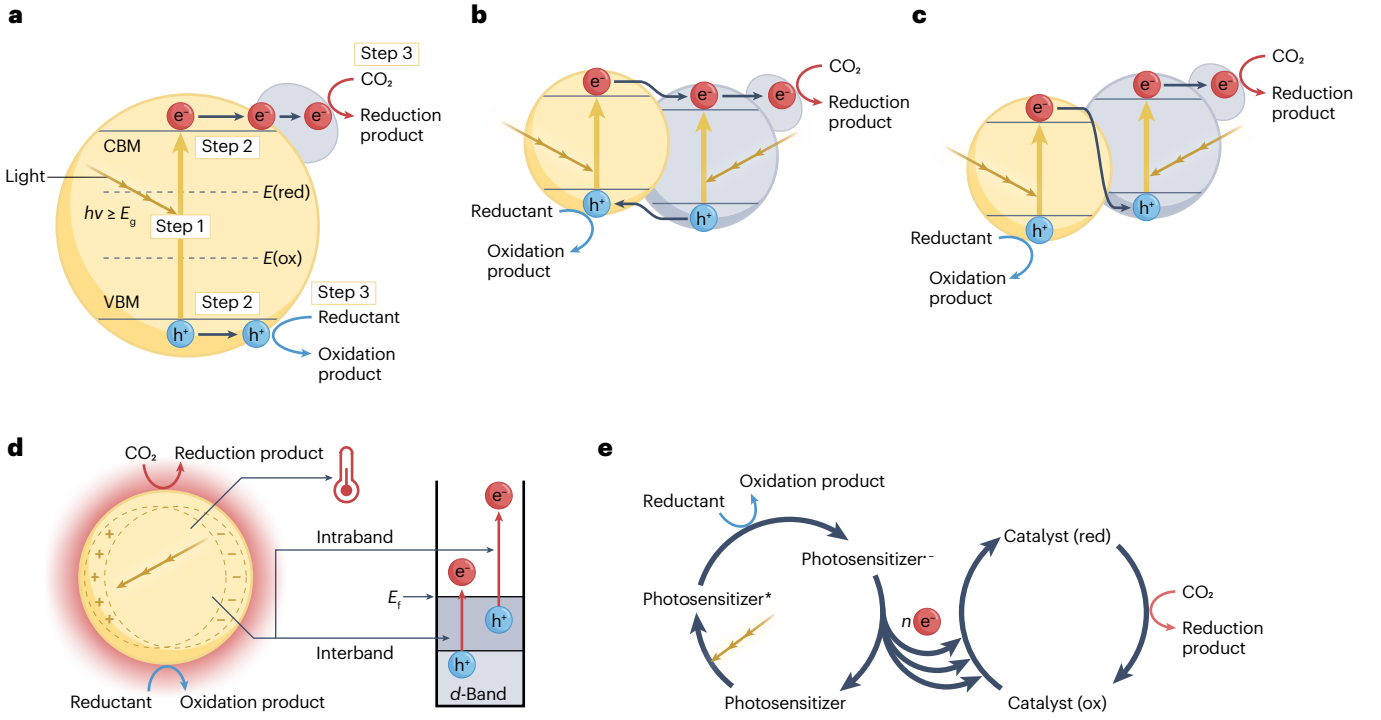

Fig. 1 | Principles of photocatalytic CO_2 reduction. Heterogeneous photocatalytic CO_2 reduction over single-semiconductor-based photocatalyst with cocatalyst (grey particle, which can be metals, carbon materials and metal complexes) (part **a**), p–n junction heterostructure photocatalyst (part **b**), *Z*-scheme heterostructure photocatalyst (part **c**) and metal-based photocatalyst with localized surface plasmon resonance effect (part **d**). Homogeneous photocatalytic CO_2 reduction over molecular catalyst with photosensitizer (part **e**). CBM, conduction band minimum; VBM, valence band maximum.

Common enzymes applied for CO_2 reduction include CO dehydrogenase and formate dehydrogenase[84–86], whose preparations require laborious purification[97,98]. Elaborately designed enzymes can be fabricated through genetic engineering and overexpression[87,88]. To eliminate the extensive purification process of isolating enzymes, bacteria cocatalysts such as *Moorella thermoacetica*[92,99] and *Sporomusa ovata*[91] have been directly used. They are purchased and inoculated in a growth medium for a certain time before assembling with the light absorber. Metal complexes can be applied as the cocatalyst for a semiconducting light absorber in heterogeneous photocatalytic CO_2 reduction[32,57–59] or an independent catalyst (namely, molecular catalyst) in homogeneous photocatalytic CO_2 reduction[32,58,100–102], whose synthesis is based on serial organic reactions[64,65].

Assembling of light absorber and cocatalyst might be a separate step following their syntheses or a simultaneous process during the synthesis of either component. As a separate step after syntheses, the assembly can be realized via wet mixing (stirring or grinding till dry)[77,80], chemical reaction[58,59,103], electrostatic coupling[94] and biopreciptation (for bacteria and enzymes)[89,90,92]. The simultaneous synthesis and assembly is beneficial for enhancing interfacial contact and thus allowing efficient charge transfer across the interface[5]. Metallic cocatalysts are typically simultaneously synthesized and assembled with the light absorber to ensure an intimate contact[5,104]. Namely, the metal ion precursor is reduced and loaded onto the light absorber using deposition techniques such as chemical deposition, photo-deposition and electro-deposition[5]. Alternatively, a three-step process of wet impregnation, calcination and reduction can be routinely used[74,105]. Similarly, graphene-based cocatalysts are generally formed in situ on a light absorber, via chemical vapour deposition or hydrothermal reaction that results in an ideal face-to-face interfacial connection[54,83]. For conventional homogeneous photocatalytic systems, the light absorber (photosensitizer) and molecular catalyst (metal complexes) are independently dispersed in the solvent[64,65]. Alternatively, molecular photosensitizer can be covalently bonded to the catalyst complex as a multinuclear supramolecular photocatalyst with linkages such as $-CH_2-CH_2-$, $-CH=CH-$, $-CH_2-O-CH_2-$ and $-CH_2-CH(OH)-CH_2-$[31,106].

Catalyst characterization

As-synthesized catalysts are characterized to clarify their structures, chemical states, optical properties and energy band positions. Catalyst properties can differ under reaction conditions, so operando characterizations are highly desirable although not readily available at present.

Structure determination. X-ray diffraction can determine the crystal structure of the catalyst and can suggest its crystallite size (up to 100 nm) according to the Scherrer equation[107]. Scanning electron microscopy (SEM) and transmission electron microscopy (TEM) can be used to assess the morphological structure of the catalyst. TEM uses higher acceleration voltages than those of SEM, resulting in smaller

de Broglie wavelengths of electrons and hence higher resolutions for lattice spacing identification[108]. Furthermore, the energy dispersive X-ray spectroscopy, electron energy loss spectroscopy and high-angle annular dark-field imaging that are available on electron microscopes allow the spatially resolved elemental analysis[109]. In addition, scanning probe microscopies such as atomic force microscopy and scanning tunnelling microscopy (STM) are widely used to reveal the thickness of 2D materials[110]. The surface area and pore volume of catalysts are measured via gas adsorption–desorption (primarily N_2) and calculated on the basis of Brunauer–Emmett–Teller theory and Barrett–Joyner–Halenda model, respectively[111]. Moreover, the adsorption–desorption of CO_2 and its temperature dependency explored via temperature-programmed desorption indicate the quantity and strength of active sites[112]. The defects and vacancies in inorganic-semiconductor-based catalysts are characterized via electron paramagnetic resonance (EPR) spectroscopy on the basis of unpaired electrons[113].

Chemical states. The chemical states of catalysts are mainly explored via spectroscopy. The chemical environment of elements is assessed by X-ray photoelectron spectroscopy (XPS) and X-ray absorption spectroscopy (XAS). The detection depth of XPS is less than 10 nm as photoelectrons generated in the bulk catalyst are highly likely to be recaptured when travelling through the sample into the vacuum[114]. By contrast, XAS offers information for both the bulk and the surface. In XAS, X-ray absorption near edge structure spectroscopy is generally used to determine oxidation states, and extended X-ray absorption fine structure spectroscopy can be used to investigate coordination and bonding properties[115]. The chemical structure of metal complex catalysts is characterized via nuclear magnetic resonance (NMR) spectroscopy and mass spectrometry (MS)[116]. The chemical structures of intermediate species formed during the synthesis of metal complexes should also be confirmed. The asymmetric vibrations of polar groups and the symmetric vibrations of nonpolar groups are detected via Fourier transform infrared (IR) spectroscopy and Raman spectroscopy, respectively, which are powerful tools to elucidate the functional groups and chemical structures of catalysts[117].

Optical properties. The characterization of optical properties is essential for photocatalysts. The wavelength-dependent light absorption ability of catalysts is measured via ultraviolet–visible (UV–Vis) spectroscopy, and the band gap can be derived from the resulting Tauc plot[118]. The behaviours of photo-generated charge carriers are studied by transient absorption spectroscopy (TAS), surface photovoltage spectroscopy (SPS), photoluminescence spectroscopy (PLS) and photoelectrochemical tests of photocurrent and electrochemical impedance spectroscopy. TAS measurements from picosecond to second timescales imply the dynamics of charge generation, recombination and interfacial charge transfer[119]. By contrast, SPS and PLS are used to solely investigate charge redistribution and charge recombination, respectively[111]. Both SPS and PLS have the steady-state and transient forms, suggesting the event count and kinetics, respectively. In addition, photocurrent and electrochemical impedance spectroscopy measured by irradiating the working electrode (coated with catalyst) can reveal the population of active charge carriers and the resistance of charge transfer in the electrode and across the electrode–electrolyte interface, respectively[29,120]. Moreover, the excited-state redox potential of photosensitizers applied in homogeneous catalytic processes can be determined by phase-modulated voltammetry[121] or using the Rehm–Weller formalism on the basis of the electron emission spectrum and ground-state electrochemical properties acquired via cyclic voltammetry[122].

Energy band positions. The energy band positions of catalysts are identified to check whether the thermodynamic requirements of photocatalytic CO_2 reduction are satisfied. The first step is to locate the Fermi level, which is generally measured as the flat-band potential versus a reference electrode by constructing Mott–Schottky plots via electrochemical tests. Generally, the Fermi level is close to CBM for n-type semiconductors and

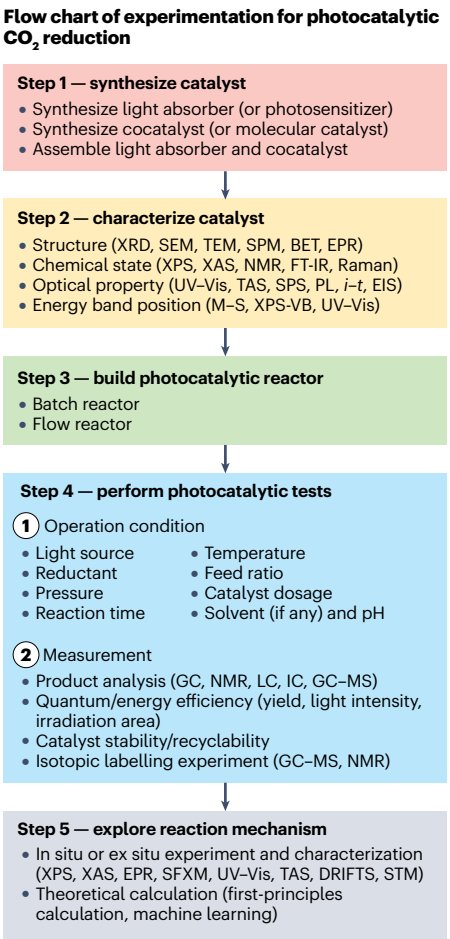

Fig. 2 | Flow chart of experimentation for photocatalytic CO_2 reduction. Step-by-step experimental procedure from catalyst synthesis and characterizations to reactor construction, photocatalytic test and reaction mechanism exploration. BET, Brunauer–Emmett–Teller surface area analysis; DRIFTS, diffuse reflectance infrared Fourier transform spectroscopy; EIS, electrochemical impedance spectroscopy; EPR, electron paramagnetic resonance; FT-IR, Fourier transform infrared spectroscopy; GC, gas chromatography; IC, ion chromatography; *i–t*, transient photocurrent measurement; LC, liquid chromatography; MS, mass spectrometry; M–S, Mott–Schottky measurement; NMR, nuclear magnetic resonance; PL, photoluminescence spectroscopy; SEM, scanning electron microscopy; SFXM, scanning fluorescence X-ray microscopy; SPM, scanning probe microscopy; SPS, surface photovoltage spectroscopy; STM, scanning tunnelling microscopy; TAS, transient absorption spectroscopy; TEM, transmission electron microscopy; UV–Vis, ultraviolet–visible spectroscopy; VB, valence band; XAS, X-ray absorption spectroscopy; XPS, X-ray photoelectron spectroscopy; XRD, X-ray diffraction.

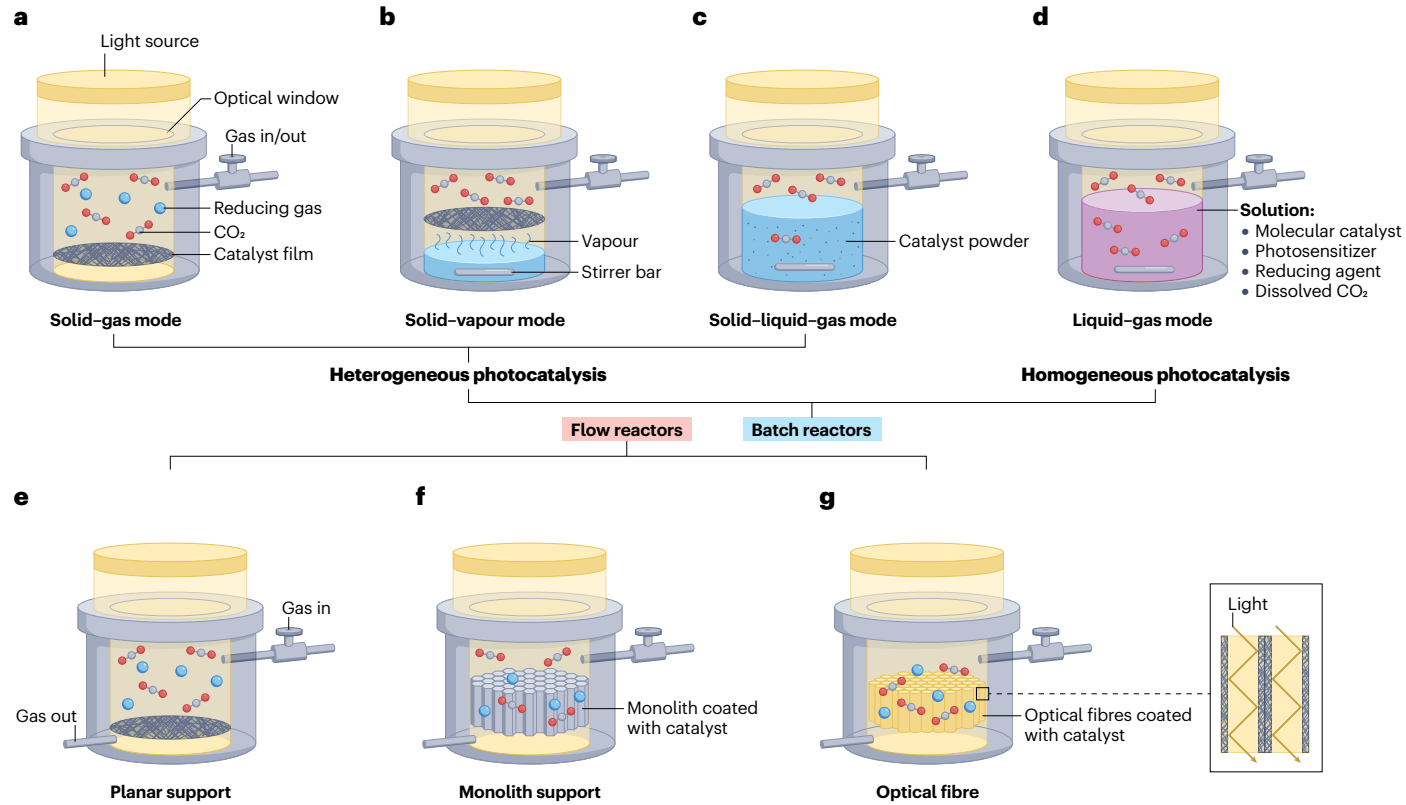

Fig. 3 | Schematic reactors for photocatalytic CO_2 reduction. Batch reactors in solid–gas mode (part **a**), solid–vapour mode (part **b**), solid–liquid–gas mode (part **c**) and liquid–gas mode (part **d**). Flow reactors with catalysts coated on planar support (part **e**), monolith support (part **f**) and optical fibres (part **g**).

VBM for p-type semiconductors, but this is not quantitative[123]. Instead, the position of VBM is determined by valence-band XPS, which is referenced to the Fermi level (zero point of binding energy). Afterward, the position of CBM is obtained on the basis of the position of VBM and the band gap derived from UV–Vis spectroscopy.

Experimental setup

The reactors for photocatalytic CO_2 reduction are categorized into batch reactors and flow reactors (Fig. 3). All reactors require an optical window that allows light irradiation on catalysts from a light source. The light sources most used in laboratories are the xenon arc lamp, mercury vapour lamp and light-emitting diode (LED) lamp. Xenon lamps offer smooth sun-like emissions from UV to visible spectra with characteristic wavelengths emitted in 750–1,000 nm. Equipping a Xenon lamp with an AM1.5-G optical filter makes a viable solar simulator and the standard light source of photocatalytic processes at a controlled light intensity of 100 mW cm^{-2}. By contrast, mercury lamps demonstrate high-intensity spectral lines emitted in deep UV to visible light regions, whereas LED lamps emit light in a very narrow band of wavelengths that is dependent on the energy band gap of the semiconductor applied to make the LED. Moreover, multiple optical filters besides AM1.5-G filter are commercially available, such as bandpass filters, longpass filters and shortpass filters. These filters provide various lights for investigating the contributions of lights with different wavelength distributions. Furthermore, it is a good choice and goal to perform field tests with utilizing natural sunlight as the light source.

Batch reactors are applicable for both heterogeneous and homogeneous reactions and are generally operated in the solid–gas mode (Fig. 3a), solid–vapour mode (Fig. 3b), solid–liquid–gas mode (Fig. 3c) or liquid–gas mode (Fig. 3d). In the solid–gas mode, the reductant is in gaseous phase (such as H_2 and CH_4), whereas in the solid–vapour mode, the reductant is in vapour phase (such as H_2O vapour). In each mode, the solid catalyst is coated on a support such as glass slide or dish[42,47,72,124], Teflon holder[78], SiO_2 disc[74,105], nickel foam[125] or aluminium plate[124]. Some supports, such as SiO_2 disc[74,105], have unique microstructures that provide a light-diffuse-reflection surface to enhance the redirection and utilization of incident light[126]. In the solid–liquid–gas mode, the reductant is in liquid phase or a solvent is present and the catalyst powder is dispersed in liquid under continuous stirring (Fig. 3c). However, this mode suffers from limited exposure of catalysts to CO_2 because of the low solubility of CO_2 in most liquids (representatively, H_2O)[78,127] and the low light utilization efficiency owing to the absorption and scattering by liquid[128]. Furthermore, homogeneous photocatalytic CO_2 reduction is performed in the liquid–gas mode, in which the solution contains molecular catalyst, photosensitizer, reductant and dissolved CO_2 (Fig. 3d).

Unfortunately, re-adsorption and back or side reactions are highly likely to occur in batch reactors, owing to the continuous accumulation of products, resulting in reduced yields[129]. By contrast, flow reactors ensure the movement of reactants and products at a constant flow rate but suffer from short residence time. Flow reactors are used for heterogeneous photocatalytic CO_2 reduction, and the inlet gas is a mixture of CO_2 and reducing gas or bubbled CO_2 through a reducing

liquid such as H_2O. The catalyst powders are coated on a support, which, from the macroscopic perspective, can be defined as a planar support (Fig. 3e), monolith support (Fig. 3f) or optical fibres (Fig. 3g). Monolith supports generally have a honeycomb structure and a high surface-area-to-volume ratio with many internal channels (Fig. 3f), enabling sufficient contact between reactants and catalyst and low pressure drop with high flow rate[130]. However, owing to the opacity of the monolith, light cannot efficiently penetrate through the long channels[128]. In addition, optical fibre can be used as a medium to uniformly and efficiently deliver light to the catalyst coated on its surface (Fig. 3g), whereas the adhesion strength of the catalyst is low and the effective surface area is small[131,132]. Inserting optical fibres into the honeycomb structure of a monolith support can address the aforementioned issues, thus being a promising architecture with hybrid supports[133,134].

Operation conditions

The operation conditions can be adjusted to optimize the photocatalytic performance. Essential operational variables include light source, temperature, reductant, feed ratio and flow rate (for flow reactors), pressure, catalyst dosage, reaction time, solvent (if any) and its pH. First, the light source represents wavelength distribution and light intensity. Wavelength distribution is tuned by using various lamps or applying various optical filters on one lamp, whereas light intensity is controlled by the output power and distance between the lamp and catalyst. Light irradiation generally causes a temperature rise. Synergetic thermo-photo catalysis with external temperature control allows operations in a wide temperature range, presenting a new way to optimizing catalytic performance[74,105]. Alternatively, for fundamental studies, the temperature rise may be suppressed by equipping an IR optical filter or adding an ice bath.

The reducing capability and affinity to catalysts vary among reductants. Furthermore, the reductant-to-CO_2 feed ratio can impact photocatalytic performance, especially selectivity. The pressures of CO_2 and reducing gas should also be considered. Although a higher pressure contributes to molecular adsorption and favours a reaction with less produced moles than converted moles, it may cause less efficient use of feedstock and some safety issues. Catalyst dosage can be adjusted to maintain a desirable catalytic efficiency. Another operation condition to consider is reaction time, which represents reaction duration for batch reactors and residence time for flow reactors. Reaction time can be optimized for an efficient forward reaction of CO_2 reduction, while suppressing backward and side reactions. Solvent should be carefully chosen on the basis of dissolving capacities for CO_2, reducing agent, catalyst, photosensitizer and products. The pH of the solvent, which directly relates to the concentration of protons, is also an important operational variable.

Furthermore, it is necessary to perform negative control experiments, namely, tests in the absence of light irradiation (at the same temperature), CO_2 (using argon instead), reductant, catalyst (leaving the blank support if used), photosensitizer or solvent. The negative control experiments should result in negligible yields. Nevertheless, to obtain solid evidence that the results are not artefacts especially when the amount of products is small, a complete and reproducible $^{13}CO_2$ labelling experiment is required.

Measurements

The assessment of photocatalytic CO_2 reduction performance requires product analysis, measurement of quantum and energy efficiencies, evaluation of catalyst stability and recyclability and confirmation by isotopic labelling experiment. Multiple products might be generated, and their quantifications involve several techniques. Gas chromatography (GC) with a thermal conductivity detector is used to detect the unreacted CO_2, produced CO and CH_4 and by-products such as H_2 and O_2. Moreover, the flame ionization detector equipped on a GC shows a high sensitivity to hydrocarbons such as CH_4, C_2H_6 and C_2H_4 and alcohols such as CH_3OH and CH_3CH_2OH. In addition, GC-flame ionization detector can quantify low-level CO and CO_2 if an Ni-catalyst-packed methanizer is installed. NMR spectroscopy with solvent suppression[35] is a powerful tool to measure liquid oxygenate products, including alcohols, aldehydes and acids[135]. The difficulty of analysing HCHO can be overcome by using a trapping agent ($NaHSO_3$)[135]. Other than NMR, liquid chromatography and ion chromatography can detect acid products such as HCOOH, CH_3COOH and $H_2C_2O_4$. Furthermore, the coupling of GC and MS provides a high accuracy for measuring almost all common products and unreacted CO_2, although the use of multiple chromatographic columns might be required[73]. In GC–MS, all substances should be properly separated; otherwise, the fragmentation patterns cannot be properly interpreted and labelling studies may lead to wrong conclusions.

Some specific measurements are needed to obtain the essential metrics for evaluating a photocatalytic CO_2 reduction process. To obtain apparent quantum efficiencies (AQEs), a series of monochromatic lights with definite wavelengths are used as the light source by equipping bandpass filters on the lamp or directly using LED lamps. The solar-to-chemical (STC) efficiency is acquired using AM1.5-G simulated sunlight. In both cases, light intensity, irradiation area and product yields should be measured. In addition, for heterogeneous photocatalysis, catalyst stability in a flow reactor can be evaluated with a long-term photocatalytic test by continuously monitoring product yields, and catalyst recyclability in a batch reactor is assessed by reusing the catalyst for multiple runs and measuring product yields for each run. The catalyst might be regenerated via washing with deionized water or heat treatment. For homogeneous photocatalysis, catalyst stability is investigated by performing tests for a long duration with product quantification at a certain time interval[64]. It is highly recommended to perform $^{13}CO_2$ labelling experiment and analyse the products by a suitable method such as GC–MS, NMR spectroscopy or Fourier transform infrared spectroscopy to confirm incorporation of ^{13}C into the product. Nevertheless, there are exemptions, given a large amount of carbon-containing substances are continuously produced in a long duration in flow reactors.

Mechanism exploration

Experimental techniques. The exploration of photocatalytic CO_2 reduction mechanisms mainly covers two aspects, namely, charge behaviours (charge generation, separation and migration) and chemical reaction pathway.

In situ XPS and XAS can detect the change in the chemical environment of catalyst elements induced by illumination or reactants, which suggests the change in electron density and the corresponding charge behaviours[24,40,136,137]. For catalysts with intrinsic or photo-induced paramagnetic responses, in situ EPR measurements can be performed alongside XPS and XAS[37,138,139]. Furthermore, the coupling of operando scanning fluorescence X-ray microscopy and environmental TEM enables the investigation of electronic structure change at the single-particle level[138]. In addition, Kevin probe and Mott–Schottky measurements reveal the Fermi level and hence the interfacial band bending upon contact[136]. For homogeneous photocatalytic CO_2 reduction, UV–Vis, XAS, TAS, IR and Raman spectroscopies help to reveal

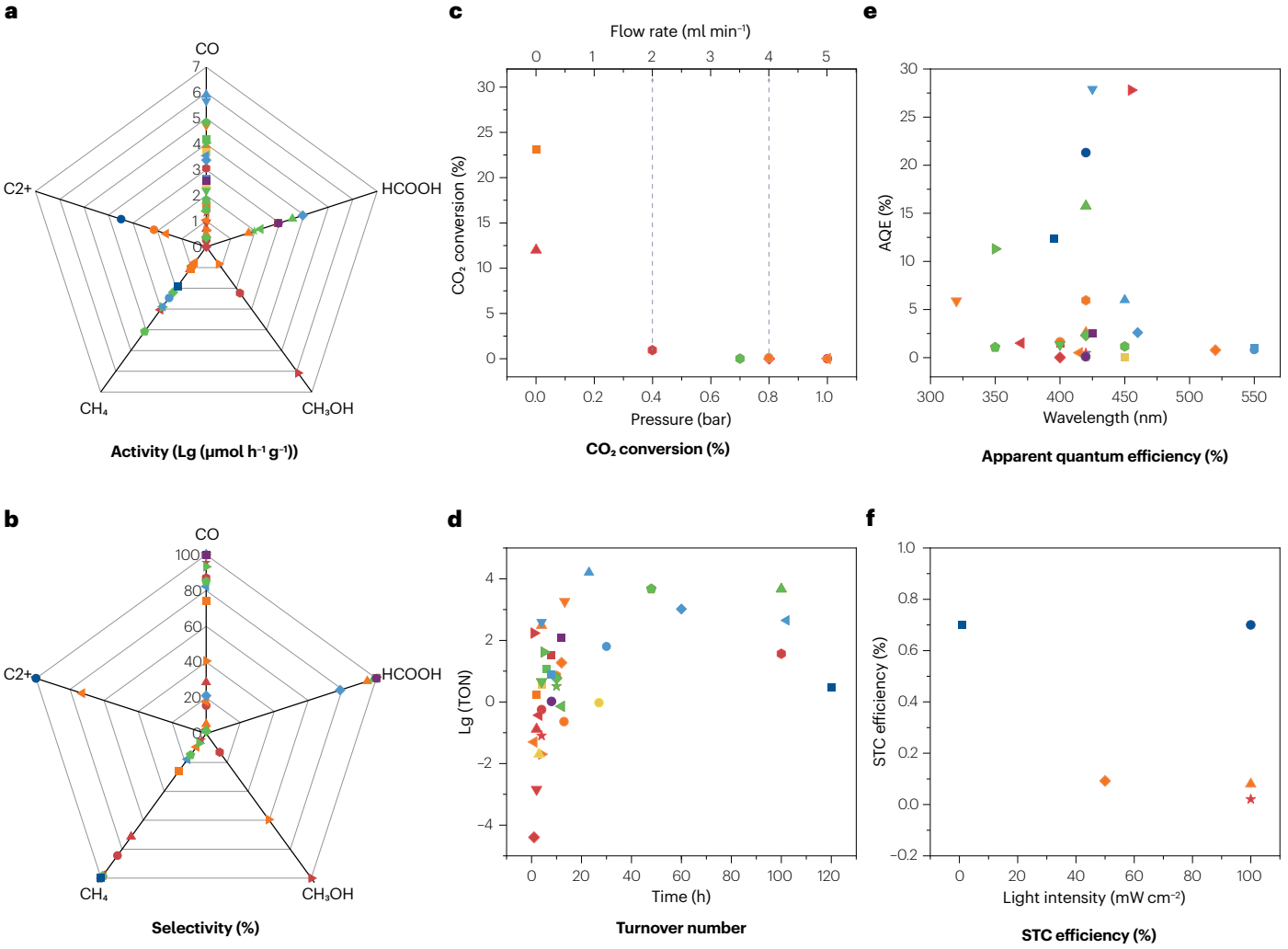

the charge transfer and electron donation and reception of the photosensitizer and molecular catalyst[64,140–142]. Furthermore, time-resolved spectroscopies are complementary to these techniques, particularly for photophysical steps and charge transfer steps.

Identifying reaction intermediates is an effective approach for depicting the chemical reaction pathway. In situ diffuse reflectance infrared Fourier transform spectroscopy is a powerful technique to detect adsorption-state intermediates and products such as monodentate carbonate (m-CO_3^{2-}), bidentate carbonate (b-CO_3^{2-}), *HCO_3, *COO, *COOH, *CHO, *CO and *OCH_3 (refs. 47,54,95,143), whereas EPR spectroscopy allows the identification of radical intermediates that are typically unstable and have an unpaired electron, such as •CO_2^-, •COOH, •CHO, •O_2^- and •OH[136,144]. Steady-state isotopic kinetic analysis can be coupled with in situ techniques to give more accurate and detailed results[143]. Moreover, advanced STM enables mechanism investigation at the single-molecule level[145]. Namely, the CO_2 dissociation process is visualized after injecting electron (electrons) from the STM tip to adsorbed CO_2, and the threshold energy for electron-induced CO_2

Fig. 4 | Literature overview of the numeric metrics in photocatalytic CO_2 reduction processes. a, Activity expressed as the logarithm of production rate per mass of catalyst. **b**, Selectivity among carbon-containing substances. **c**, CO_2 conversion rate (versus pressure for batch reactors; versus flow rate for flow reactors). **d**, Turnover number (TON) in the logarithm form. **e**, Apparent quantum efficiency (AQE). **f**, Solar-to-chemical (STC) efficiency. Metal-oxide-based catalysts (red symbols): Cu_2O-Pt/SiC/IrO_x (ref. 22); Pt/SiO_2-TiO_2 (ref. 42); Pd/HPP-TiO_2 (ref. 70); $CsPbBr_3/TiO_2$ (ref. 211); Mn,C-ZnO[44]; Cu_2O-ZnO[212]; Cu_2O[138]; $In_2O_{3-x}(OH)_y$ (ref. 45) and Bi_3TiNbO_9 (ref. 159). Other inorganic-semiconductor-based catalysts (orange symbols): Au/CdS[72]; C-SnS_2 (ref. 46); CotpyP/$SrTiO_3$:La,Rh|Au|RuO_2/$BiVO_4$:Mo[20]; Rh/$SrTiO_3$ (ref. 181); $CuIn_5S_8$ (ref. 47); $AgInP_2S_6$ (ref. 156); $Pb_{0.6}Bi_{1.4}O_2Cl_2$ (ref. 49) and Gersiloxene[56]. Metal-based catalysts (yellow symbols): Au[24]; BiH_x (ref. 25) and SiH_x (ref. 33). MOF/COF-based catalysts (green symbols): Ni/MOF[36]; Co/MOF[213]; Ir/MOF[35]; Ru/MOF[214]; Cu-Ni/MOF[150]; MOF–COF[40]; TiO_2/MOF[37]; CdSe/CdS-COF[39]; $Ru(phen)_3$/Eu-MOF[139] and metalorganiczyme (monolayered MOF-based artificial enzyme)[38]. Molecular catalysts (light blue symbols): Zn-TPY-TTF[73]; Pt/Zn-TPY-TTF[73]; Cu-PP/Fe-TDHPP[63]; Ir-QPY/Co-Pc[160]; $Ru(phen)_3$/Co-QPY[65] and Fe-p-TMA[64]. Bacteria-based catalysts (dark blue symbols): M.b-NiCu-CdS[90] and S.o/Cr_2O_3/$SrTiO_3$:La,Rh|RuO_2/$BiVO_4$:Mo[91]. Enzyme-based catalysts (purple symbols): PSP/TPY[87] and CdS/$CsgA_{A7}$-FDH[89]. COF, covalent organic framework; FDH, formate dehydrogenase; HPP, hyper-crosslinking porphyrin-based polymer; MOF, metal–organic framework; PSP, photosensitizer protein; QPY, quaterpyridine; TDHPP, tetrakis(dihydroxyphenyl)-porphyrin; TMA, trimethylanilinium; TPY, terpyridine; TTF, tetrathiafulvalene.

dissociation is acquired by analysing bias-dependent dissociation yields. Furthermore, the thermodynamic parameter, reaction order, influence of diffusional step on kinetics and role of proton donor are also important for understanding reaction pathway.

For plasmonic catalysis, there is one more essential task, namely, identifying the thermal and hot-carrier contributions in the catalytic process. This can be achieved by exploring the dependences of reaction rate and quantum efficiency on light intensity, comparing the kinetic isotope effects under illumination and in dark, and electron quenching, in combination with some advanced in situ characterization techniques[146,147].

Theoretical calculations. First-principles computational chemistry, especially density functional theory (DFT), is most widely used to explore the photocatalytic CO_2 reduction mechanism. DFT calculations are performed on pristine catalysts to identify band structure and electronic excitation. Furthermore, DFT can predict the interactions between the catalyst and CO_2, intermediates or products to determine parameters such as the adsorption geometry and energy, change in Gibbs free energy, transition state, reaction barrier and rate-determining step[73,148–150]. Van der Waals correction and spin polarization are used for accurately modelling the system, and the solvation model is needed if solvent is involved[49]. Besides, the light irradiation effect is modelled via the time-dependent DFT method or kinetic Monte Carlo simulation[151,152]. All possible paths should be considered, calculated and compared on the basis of both thermodynamics (Gibbs free energy) and kinetics (energy barrier of the transition state)[45,150].

Machine learning, as an emerging data-driven computational method for modelling and interpreting complicated multidimensional relations, has been adopted as a complement of the time-intensive and resource-intensive first-principles calculations[153]. Machine learning is used to screen elementary steps and preclude the pathways involving steps predicted to have extremely high barriers[154,155]. However, current application of machine learning techniques is still limited, owing to the lack of sufficient data[153].

Results

There are six important numeric metrics in photocatalytic CO_2 reduction processes that should be obtained and reported, including the production rate, selectivity, CO_2 conversion rate, turnover number (TON) or turnover frequency (TOF), (apparent) quantum efficiency and STC efficiency. Figure 4 summarizes these numeric metrics of 40 photocatalysts from 7 groups to illustrate the general results of interest and the best practice (among these studies). Each metric is discussed in detail in the corresponding section regarding its calculation, analysis and optimization. When optimizing the operation condition, one should have an overall view of all facets of the performance by considering a matrix of metrics. For example, applying a large light intensity might enhance the production rate, CO_2 conversion rate and TON (TOF) but reduces quantum efficiency and STC efficiency. In addition, catalyst stability in a long-term run and catalyst recyclability that allows multiple runs are also essential metrics. Furthermore, the most common mechanisms of photocatalytic CO_2 reduction are elucidated at the end of this section.

Production rate

Production rate describes catalytic activity. Taking the effectiveness of time and material into account, production rate is calculated via equation (1) with a recommended unit of $\mu mol\ h^{-1}\ g_{cat}^{-1}$.

$$\text{Production rate}\ (\mu mol\ h^{-1}\ g_{cat}^{-1}) = \frac{\text{Yield over a period of time}\ (\mu mol)}{\text{Time}\ (h) \times \text{Mass of catalyst}\ (g)} \quad (1)$$

This metric is best suited for heterogeneous systems but can be applied to all photocatalytic CO_2 reduction processes. TON and TOF are preferred for homogeneous systems as the exact number of active sites is known. Comparison between homogeneous and heterogeneous systems remains challenging. As shown in Fig. 4a, CO is the most common product of CO_2 reduction, with a wide range of production rates from 1 $\mu mol\ h^{-1}\ g_{cat}^{-1}$ to ~10^6 $\mu mol\ h^{-1}\ g_{cat}^{-1}$. Moreover, some photocatalysts contribute to the production of HCOOH and CH_4, whereas the production rates are generally less than ~10^4 $\mu mol\ h^{-1}\ g_{cat}^{-1}$. In addition, CH_3OH and multicarbon substances (such as C_2H_4 (ref. 156), CH_3CHO[46] and CH_3COOH[91]) are formed over some inorganic-semiconductor-based photocatalysts, most of which are at the rate of 10~10^4 $\mu mol\ h^{-1}\ g_{cat}^{-1}$ except CH_3OH production over Cu_2O catalyst[138]. Furthermore, this plot suggests the higher activity of molecular catalysts and enzymes than others towards the generation of carbon-containing substances. The plasmonic catalysts also demonstrate impressive production rates, whereas large light intensities are commonly used.

Production rate can also be expressed as the areal activity to illustrate the effectiveness of irradiation area and can be calculated via equation (2):

$$\text{Production rate}\ (\mu mol\ h^{-1}\ cm_{cat}^{-2}) = \frac{\text{Yield over a period of time}\ (\mu mol)}{\text{Time}\ (h) \times \text{Irradiation area on catalyst}\ (cm^2)} \quad (2)$$

This metric is very meaningful when the catalyst itself exhibits as a film or powdered catalyst is coated on a substrate towards promising solar panel technologies for STC conversion[157]. To improve the production rate, the number of active sites and activity of each active site should be enhanced, which require an elaborate design of catalysts.

Selectivity

Selectivity towards high-value products is desired in terms of economic and environmental benefits. A high selectivity (preferentially 100%) also eliminates or reduces the energy consumption and cost for separating and purifying products. Selectivity is defined as the ratio of the yield of a target product to the sum of the yields of all products (equation (3)):

$$\text{Selectivity} = \frac{\text{Yield of target product (μmol)}}{\text{Yields of all products (μmol)}} \quad (3)$$

The products typically represent the carbon-containing substances resulting from CO_2 reduction. H_2 should also be accounted for if water or other proton source is used as the reductant or reaction medium. Figure 4b summarizes the selectivity among carbon-containing substances, suggesting the realization of inspiring selectivity of 100% for various products[22,24,36,40,47,158]. Nevertheless, simultaneous generation of multiple products with limited selectivities is still a common phenomenon (particularly, CO and CH_4)[37,70,159]. Besides, selective production of multicarbon species remains a huge challenge over the currently dominant C1 chemicals. Moreover, the competitive H_2 evolution reaction further limits the selectivity in numerous studies[63,65,73,160].

Catalytic selectivity highly depends on the interactions between the molecule and catalytically active site[16,64]. It is hard to clarify which group of catalysts shows higher selectivities. Organic-related catalysts (MOFs, COFs, molecular catalysts, bacteria and enzymes) and low-dimensional inorganic catalysts have more defined and modulable molecular structures that allow the precise control of active sites, thus more likely to realize high selectivities. However, it remains a challenge to achieve the reduction of CO_2 beyond two electrons.

CO_2 conversion rate

The CO_2 conversion rate is a critical metric that has not received much attention, but should be included as an essential metric in the assessment of photocatalytic CO_2 reduction systems. It reflects the effectiveness of CO_2 feedstock utilization, which is calculated via equation (4):

$$\text{CO}_2\text{ conversion rate} = \frac{\text{Amount of reacted CO}_2\text{ (μmol)}}{\text{Amount of fed CO}_2\text{ (μmol)}} \quad (4)$$

Besides the nature of the catalyst, the CO_2 conversion rate is also affected by the total amount of available CO_2, reaction time for batch reactors and CO_2 flow rate for flow reactors. The CO_2 conversion rate should be calculated when chemical equilibrium is reached. Currently, most processes demonstrate tiny CO_2 conversion rates less than 1% as a large substrate access is provided to the systems. CO_2 conversion rates higher than 10% have been attained using low-concentration CO_2 feedstock at 300–1,000 ppm over inorganic-semiconductor-based photocatalysts as important practices towards CO_2 conversion in air[70,72] (Fig. 4c). Ultimately, close-to-unity conversion rates are desirable to avoid energy penalties and CO_2 release into the atmosphere.

Turnover number and frequency

TON (equation (5)) and TOF (equation (6)) are two important metrics to quantify the catalytic activity of each active site. To reflect the real rate of catalytic systems, TOF may be derived from the slope of the TON–time curve instead of the mean value over the whole duration:

$$\text{Turnover number} = \frac{\text{Number of reacted CO}_2}{\text{Number of active sites}} \quad (5)$$

$$\text{Turnover frequency (h}^{-1}\text{)} = \frac{\text{Number of reacted CO}_2}{\text{Number of active sites} \times \text{Time (h)}} \quad (6)$$

For homogeneous catalytic systems with molecular catalysts, the number of active sites is well defined. However, for heterogeneous catalytic systems, the identification and quantification of active sites are challenging. As an approximation, cocatalyst such as metal nanoparticle is generally regarded as active site. As summarized in Fig. 4d, most TONs were measured in a short period of time (<15 h) with a wide distribution from 10^{-5} to 10^3. Long-term measurements up to 120 h were performed for some catalysts, demonstrating larger TONs from ~1 to 10^4. Moreover, molecular catalysts seem to be more active with larger TONs and TOFs than other catalysts, owing to their effective utilization. For example, the Cu-PP/Fe-TDHPP catalyst realized an impressive TON of 16,109 and TOF of 700 h^{-1} (ref. 63).

Quantum efficiency

Quantum efficiency (or quantum yield) is an essential numeric metric to describe the effectiveness of converting photons into active electrons that participate in reactions. There are two quantum efficiencies, namely, internal quantum efficiency based on absorbed photons by catalyst and external or apparent quantum efficiency (EQE or AQE) based on incident photons. Although internal quantum efficiency better illustrates the intrinsic properties of catalysts, EQE (AQE) is of greater practical significance and easier to measure, thus having been widely used to evaluate photocatalytic processes. Equation (7) illustrates the classic formula and convenient formula for EQE (AQE) calculation, in which the number of electrons required to reduce CO_2 is 2 for CO, HCOOH and $H_2C_2O_4$, 4 for HCHO, 6 for CH_3OH, 8 for CH_4 and CH_3COOH, 10 for CH_3CHO, 12 for C_2H_5OH and C_2H_4 and 14 for C_2H_6.

$$\begin{aligned}&\text{Apparent quantum efficiency}\\ &= \frac{\text{Number of electrons for CO}_2\text{ reduction}}{\text{Number of incidentphotons}}\\ &= \frac{\sum(\text{Number of produced } x \text{ molecule} \times \text{Number of electrons required to reduce CO}_2\text{ to } x)}{\text{Light intensity (W m}^{-2}) \times \text{Irradiation area (m}^2) \times \text{Time (s)} \div \frac{\text{Planck constant (J s)} \times \text{Light speed (m s}^{-1})}{\text{Wavelength (m)}}}\\ &= \frac{33.2296 \times \sum[\text{Yield of } x \text{ (μmol)} \times \text{Number of electrons required to reduce CO}_2\text{ to } x]}{\text{Light intensity (mW cm}^{-2}) \times \text{Irradiation area (cm}^2) \times \text{Time (h)} \times \text{Wavelength (nm)}}.\end{aligned} \quad (7)$$

Figure 4e illustrates the wavelength-dependent AQEs for various catalysts. Although most AQEs remain less than 10%, significant AQEs up to ~28% in the visible-light range have been reported over Cu_2O[138] and Ir-QPY/Co-Pc[160] catalysts. To improve AQE, the catalyst should demonstrate broad and intense light absorption, and photo-generated charge carriers can be efficiently separated and migrated to induce surface reactions.

Solar-to-chemical efficiency

STC efficiency is utilized to quantify the efficiency of energy conversion from solar energy to stored chemical energy (equation (8)):

$$\text{Solar-to-chemical efficiency} = \frac{\sum [\text{Yield of } x\ (\mu\text{mol}) \times \text{Gibbs free energy change of reducing } CO_2 \text{ to } x\ (\text{kJ mol}^{-1})]}{\text{Light intensity } (\text{mW cm}^{-2}) \times \text{Irradiation area } (\text{cm}^2) \times \text{Time } (\text{s})} \quad (8)$$

The sum of the Gibbs free energy change of reactions should be positive to provide a positive value for STC efficiency. Photocatalytic CO_2 reduction processes with sacrificial reagents (strong reductants) do not have valid (positive) STC efficiencies as the chemical energy is released but not stored under illumination. Unfortunately, only a small number of papers have reported the STC efficiencies, which are less than 1% (Fig. 4f), far from the industrial requirement. The same strategies to improve AQE can be used to enhance STC efficiency.

To reflect the economic value of a solar chemical process, an alternative value-oriented metric of solar-to-value rate can be reported by subtracting the total cost of reactants from the total value of products per unit time per unit irradiation area (considering practical solar utilization) (equation (9)):

$$\text{Solar-to-value rate} = \frac{\sum [\text{Value of } x\ (\$\ \mu\text{mol}^{-1}) \times \text{Yield of } x\ (\mu\text{mol})] - \sum [\text{Cost of } y\ (\$\ \mu\text{mol}^{-1}) \times \text{Consumption of } y\ (\mu\text{mol})]}{\text{Time } (\text{h}) \times \text{Irradiation area } (\text{cm}^2)} \quad (9)$$

The cost of CO_2 is negative owing to carbon taxes, whereas the costs of most sacrificial reagents are much higher than the values of CO_2 reduction products and the oxidation product of the sacrificial reagent. The solar-to-value metric may be expanded with including the costs of feedstock pre-treatment, product collection and separation, catalyst preparation, and scaling factors. This requires a comprehensive techno-economic analysis.

Catalyst stability and recyclability

An ideal catalyst for photocatalytic CO_2 reduction can maintain its excellent performance for a long time in terms of both activity and selectivity. On the one hand, it exhibits a high stability in a long-term run lasting tens to hundreds of hours. On the other hand, it shows a great recyclability that allows multiple runs, especially for batch reactions. The duration and cycle index are typically within 20 h and 3, respectively, which are still below a rigorous stability test[161,162]. Furthermore, characterizing the spent catalyst is essential to confirm the robustness of the catalyst and to help to understand the reasons for catalyst deactivation (if any).

Photocatalytic mechanism

Photon absorption and subsequent charge transfer can promote the photocatalyst and other components in the system to the excited state. The molecules reconfigure to accommodate the excited-state potential energy surfaces, driving the chemical transformation with lower activation barriers[18]. The excited state cannot simply be described using the ground-state theory and characterizations, so a thorough understanding of the excited-state dynamics is the key to exploring the photocatalytic mechanism.

The mechanism of photocatalytic CO_2 reduction is typically expressed in terms of charge behaviour and reaction pathway. The charge transfer directions among the light absorber, cocatalyst and reactants are highly dependent on energy band position, photon energy, molecular adsorption and redox potential. After elucidating the charge transfer directions, heterostructure catalysts can be identified as p–n junction or *Z*-scheme, both of which allow more efficient charge separation than their single components[5]. The most common reaction routes of heterogeneous photocatalytic CO_2 reduction to C1 products are summarized in Fig. 5, including the oxygen-atom-connecting monodentate or bidentate intermediate route with the direct protonation of CO_2 by H^+ from solution or CO_2 insertion into X–H bond[1] (Fig. 5a); the surface-bound bicarbonate intermediate route via the reaction between CO_2 and surface -OH group[163] (Fig. 5b); the $\bullet CO_2^-$ radical intermediate route with the following formaldehyde pathway or carbene pathway[164] (Fig. 5c) and the glyoxal intermediate route in which the dimerization of *CHO into glyoxal is followed by sequential reactions to form *CH(OH)(CHO), CH_2(OH)(CHO), *CH_2(CHO), CH_3CHO, *CO(CH_3), CO + *CH_3 and CH_4 (ref. 1) (Fig. 5d). For the formation of multicarbon products, C–C coupling is the key step. For example, pathways towards C_2H_4 and C_2H_6 go through coupling of *CH_2 and *CH_3 intermediates (carbene pathway), whereas the coupling of *CHO intermediates (glyoxal pathway) can produce various C1 and C2 oxygenates[165]. The mechanisms of homogeneous photocatalytic CO_2 reduction are quite different, and η^1-CO_2 adduct and hydride complex are believed the most common intermediates[30].

It should be noted that theoretical calculations cannot really predict or demonstrate the photocatalytic mechanism. Firstly, the complex photocatalytic CO_2 reduction system cannot be rigorously modelled, especially for light irradiation, catalyst structure and solvation effect. Secondly, current calculation methods are not yet able to accurately model the energy surfaces to find the free energy reaction pathways in excited states. Therefore, the calculation results should only serve as an auxiliary reference of experimental results.

Applications

Currently, photocatalytic CO_2 reduction is mainly pursued in academic laboratories, but it may be ultimately applied to valourize atmospheric CO_2, emission streams from thermal power stations and iron factories, and exhaust gases of vehicles[166]. In this section, the considerations for practical application of photocatalytic CO_2 reduction are discussed together with a few examples of application.

Considerations for practical application

There are seven major considerations for the practical application of photocatalytic CO_2 reduction processes. The first consideration is the CO_2 source, which is normally atmosphere and emission streams[166,167]. Different CO_2 sources have different CO_2 concentrations down to ppm level and different interfering species (such as O_2, N_2, SO_2 and H_2O) that might compete with CO_2 for molecular adsorption and chemical reactions[49,70,72]. Therefore, additional processes of CO_2 capture and purification before photocatalytic reactions might be needed.

The second consideration is the availability of solar energy because only in sunny daytime can solar energy be utilized to drive reactions[18]. In addition, sunlight intensity varies with location and weather, so solar concentrators might be installed[124]. The limited solar energy only allows for intermittent operations[73] unless solar energy is stored as electric energy in the daytime, which then provides illumination via lamp at night[18,168]. A persistent photocatalytic system was recently proposed to store charges in a capacitor or battery-like material that interfaces with a photocatalyst during illumination and discharge after illumination to continue driving a catalytic reaction[169].

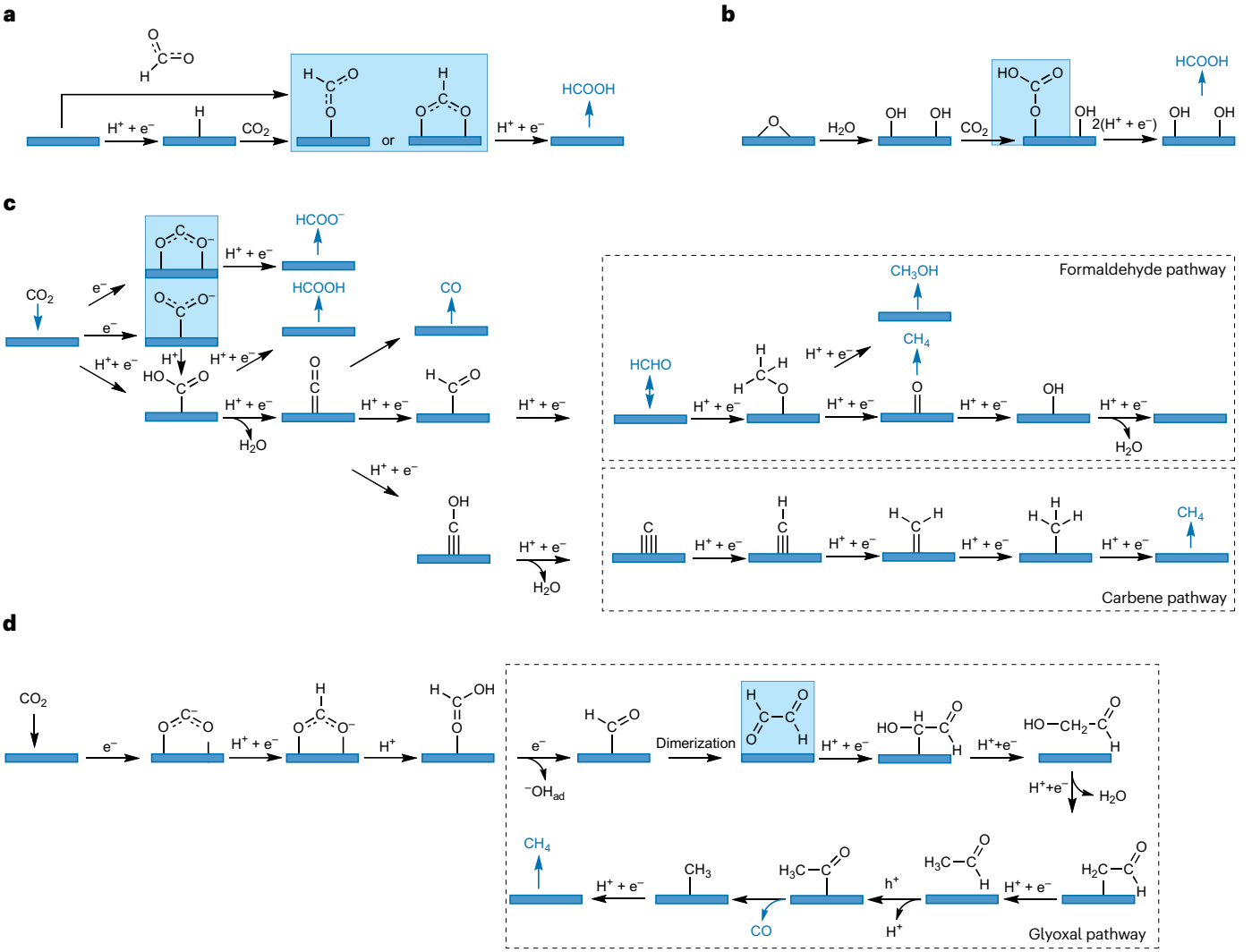

Fig. 5 | Possible routes of heterogeneous photocatalytic CO_2 reduction reaction. a, Monodentate or bidentate intermediate route. **b**, Surface-bound bicarbonate intermediate route. **c**, $\bullet CO_2^-$ radical intermediate route with the following formaldehyde pathway and carbene pathway. **d**, Glyoxal intermediate route. The important intermediates are highlighted in light blue.

The third consideration is the scale-up of the photocatalytic reactor. As mass and photon transfers are highly dependent on scale, the optimal reactor geometry, window material and thickness and catalyst architecture in bench-scale tests might not be applicable for a large scale[8,170]. Accurately modelling mass, photon and heat transfers for optimizing large-scale reactors is a promising approach to address this issue[8,171].

The fourth consideration is the separation and collection of products. There is often a mixture of products, and reactants (CO_2 and reductant) are not fully consumed, requiring the separation for downstream utilization. The installation and operation of separation systems such as membrane system and extraction system would lead to additional cost and energy consumption. Developing a tandem reaction system to utilize products on site is another solution[172,173].

The fifth consideration is cost-effectiveness, which is evaluated through techno-economic assessment on the basis of modelling of detailed processes with rational boundary conditions[8,167,174]. Non-technical factors that determine economic viability such as up-to-date political framework, supply chain partnership, consumer behaviour and labour force optimization should be considered as well[175]. The result should be compared with those of other CO_2 capture and utilization technologies.

The sixth consideration is environmental impacts, which are quantified via life cycle assessment following ISO Standard 14040/14044 series[176]. Life cycle assessment mainly covers fossil fuel depletion, global warming potential, ozone depletion, smog formation, acidification, eutrophication, ecotoxicity and human health[176,177].

The last consideration for the scale-up of photocatalytic CO_2 reduction processes is the system life span, which directly influences the economic and environmental benefits. The cost, labour and environmental impacts associated with system maintenance and upgrading should be accounted as well.

Application examples

Photocatalytic CO_2 reduction has been applied to several chemical processes, although they remain at the laboratory stage. The sunlight-driven reduction of CO_2 by H_2O is the most attractive application for realizing scalable energy storage and carbon-neutral production of high-energy-density fuels with O_2 as the only by-product[178,179]. Moreover, photocatalytic CO_2 reforming of CH_4 is an essential application that allows the simultaneous treatment of two primary greenhouse gases with producing syngas as a versatile chemical feedstock[105,175,180,181]. Even ambient light irradiation can lower the reaction temperature by ~200 °C while maintaining similar efficiency relative to the thermal catalytic process[105]. Furthermore, photocatalytic CO_2 hydrogenation shows a great promise as the green alternative to conventional thermal catalytic reverse water–gas shift reaction, Sabatier reaction, as well as Fischer–Tropsch processes[6,45,182].

Current attempts towards the practical application of photocatalytic CO_2 reduction are mainly focused on the direct utilization of air as CO_2 feedstock[70,183,184] or natural sunlight as light source[73], whereas the reactors are still in bench scale. Inspiringly, a modular 5-kW pilot-scale solar-thermal catalytic system has been developed, which directly captured CO_2 and H_2O from ambient air and converted them to syngas first and further to drop-in fuels such as CH_3OH and kerosene under field conditions[185]. This setup is a valuable reference for practical photocatalytic CO_2 conversion, although it ran via thermal catalysis so far. To apply for photocatalysis, slight modifications on the paraboloidal concentrator and replacement of catalyst are desired.

Reproducibility and data deposition

Data reporting and deposition are not standardized, and reproduction of results across the field of photocatalytic CO_2 reduction remains a challenge. This section discusses the factors affecting reproducibility, summarizes the data reporting requirements and proposes standard operation condition for comparing catalytic performances.

Factors affecting reproducibility

First, the reproducibility is highly dependent on the structure and properties of catalysts. In heterogeneous photocatalytic CO_2 reduction processes, the crystal phase, particle size, morphology, exposed facets and defects of catalysts directly influence CO_2 adsorption, light absorption, charge separation and reaction pathway, hence photocatalytic efficiency[42,47,95,138,186]. Among these, defects are the most under-rated yet the most important as they might cause up to tenfold reduction in activity and quite different selectivities[35,45,47,95,96]. In homogeneous processes, the exact structure and high purity of the molecular catalyst and photosensitizer must be ensured.

The carbon-based catalysts themselves or carbonaceous residues on the catalyst surface (resulting from catalyst preparation or adsorption of atmospheric volatiles) would impact the yield of carbon-containing substances[19,187]. For example, these carbon-based catalysts or carbonaceous residues might serve as the carbon feedstock for generating carbon-containing substances, rather than CO_2 reduction. Furthermore, carbonaceous residues can cover the active sites on the catalyst surface, thus inhibiting the adsorption and subsequent photocatalytic reduction of CO_2.

The shape, size and material of photocatalytic reactors directly affect mass, heat and photon transfers[8,170], leading to different results. Although some photocatalytic reactors have been commercialized, many researchers use home-made reactors. However, most reports simply present a scheme or photo of the reactor without detailed description of its dimensions and materials for walls and optical window, making it hard to reproduce the results.

The photocatalytic efficiency is strongly correlated to the light source. Different light sources have different spectra and intensities, providing photons with different energies in different quantities. The absorbed photons further determine the number of excited charge carriers for driving photocatalytic reactions[18]. Even for the same lamp, the spectrum and intensity will change with time.

Reporting requirements

Comprehensiveness and transparency are crucial for data reporting and deposition. The necessary data associated with photocatalytic CO_2 reduction and their definitions, reporting requirements and reporting format regarding experimentation, catalyst characterization, photocatalytic performance, reaction mechanism and carbon origin confirmation are elaborated in Table 2. First, a comprehensive and detailed description of experimental procedures and setups is of vital importance to ensure the reproducibility. Particularly, a scheme or photo of the reactor should be provided with annotations on its dimensions and materials; and the model, spectrum and intensity of the light source should be reported. In addition, the reaction temperature should be in situ probed via thermocouple or IR thermal imager. Moreover, the reporting of photocatalytic performance is based on seven metrics including production rates and selectivities of all products, CO_2 conversion rate, TOF, AQEs at various wavelengths, STC efficiency and catalyst stability or recyclability. All metrics should be reported as the mean value with standard deviation derived from at least three parallel tests. Also, it is necessary to elucidate the origin of the carbon in products by isotopic labelling experiment with $^{13}CO_2$, negative control tests and carbon balance calculation. Finally, schematic illustrations of the charge behaviours, energy band positions of catalyst, redox potentials and chemical reaction pathway should be supplied on the basis of experimental evidence. In addition, it is highly desired that the contributions of hot charge carriers and thermal energy in plasmonic catalytic processes can be distinguished.

Recommended catalytic performance evaluation

Although the optimization of operation conditions is encouraged, the results obtained under the standard operation condition should also be provided to compare data from different laboratories. The standard operation condition is proposed as follows: 100 mW cm^{-2} AM1.5-G simulated sunlight applied as the light source, with the temperature monitored and reported (but not controlled) to simulate practical conditions. In terms of catalyst loading, 10-mg catalyst in 30-ml solvent (if required) is suggested. For batch reactors, 1-atm CO_2 is suggested, whereas for flow reactors, a flow rate of 10 ml min^{-1} CO_2 should be used. The reductants have diverse chemical natures and phases, with a recommended dosage of 1 atm or 10 ml min^{-1} for gas reductants (such as H_2 and CH_4); 30 ml for liquid reductants (such as H_2O) or 20% volume fraction for solvate reductants (such as triethylamine). The reaction time for batch reactors is 2 h, and flow reactors should operate until stable activity is attained.

Limitations and optimizations

At present, photocatalytic CO_2 reduction suffers from two main limitations, namely, low energy conversion efficiency and low product selectivity. In addition, many systems, especially homogeneous photocatalytic systems, use expensive sacrificial reagents. This section focuses on the low energy conversion efficiency and product

Table 2 | Data reporting required for photocatalytic CO_2 reduction

Data	Definition and reporting requirement	Reporting format
Reporting of experimentation		
Chemicals and materials	Manufacturer, product number and purity of all chemicals and materials	Description
Catalyst synthesis	Detailed step-by-step procedure of catalyst synthesis	Description
Catalyst characterization	Instrument model and test condition applied for catalyst characterizations	Description
Experimental setup	Scheme or photo of experimental setup with annotations on its dimensions and materials; model, spectrum and intensity of light source	Figure, description
Photocatalytic test	Detailed operation steps and conditions (pressure, feed ratio, catalyst dosage, in situ probed temperature and reaction time) of photocatalytic CO_2 reduction	Description
Product analysis	Apparatus (model, column and detector), test condition (temperature, carrier gas or solvent and flow rate) and calibration curve applied for product analysis	Description
Reporting of isotopic labelling results		
Isotopic labelling results	Photocatalytic test with $^{13}CO_2$ and subsequent product analysis via GC–MS and NMR with the spectra presented	Figure, description
Reporting of photocatalytic performance		
Production rate (all products)	Yield of a product per unit time per unit mass of catalyst	Numeric ($\mu mol\,h^{-1}\,g^{-1}$)
Selectivity (all products)	Ratio of the yield of a product to the sum of the yields of all products	Numeric (%)
CO_2 conversion rate	Ratio of the amount of reacted CO_2 to the amount of supplied CO_2	Numeric (%)
Turnover frequency	Number of CO_2 molecules converted per active site per unit time	Numeric (h^{-1})
Apparent quantum efficiency (various wavelengths)	Ratio of the number of electrons participating in CO_2 reduction reactions to the number of incident photons	Numeric (%), figure
Solar-to-chemical efficiency	Ratio of the stored chemical energy to incident solar energy	Numeric (%)
Catalyst stability	Capability of the catalyst to maintain its activity in a long-term run	Figure
Catalyst recyclability	Capability of the catalyst to maintain its activity in multiple runs	Figure
Experimental uncertainty	Mean value and standard deviation calculated with more than three parallel catalytic tests	Error, error bar
Reporting of other essential data		
Catalyst information	Composition, structure, optical absorption and energy band positions of catalyst; characterizations of the spent catalyst if deactivation occurs in the long-term run	Figure, description
Photocatalytic mechanism	Experimental evidence and schemes of charge behaviours and reaction pathway	Figure, description
Negative controls	Tests in the absence of light irradiation, CO_2, reductant, catalyst or solvent and subsequent product analysis	Numeric
Mass balance of carbon	Comparison of the amounts of carbon before and after photocatalytic tests	Numeric

GC–MS, gas chromatography–mass spectrometry; NMR, nuclear magnetic resonance.

selectivity in terms of their causes and optimization strategies, which are summarized in Box 1.

Low energy conversion efficiency

One of the main barriers of facilitating the industrial application of photocatalytic CO_2 reduction is its low energy conversion efficiency (usually <1%), which has three main causes. First, the utilization of solar energy is limited by the poor absorption of visible and IR lights by catalyst, parasitic light loss and light intensity gradient[7,188]. Second, CO_2 is difficult to be activated, owing to its stable linear symmetric structure with an average C = O bond energy up to 750 kJ mol^{-1} (ref. 18). Third, multiple proton-coupled electron transfers that are involved in photocatalytic CO_2 conversion (as illustrated in Fig. 5) suffer from sluggish kinetics[16].

Energy conversion efficiency can be optimized from three aspects. The first one is exploiting catalysts with sufficient active sites, wide solar-spectrum absorption and efficient charge separation. Defect engineering is an effective strategy that not only provides more sites for CO_2 adsorption but also enhances light harvesting, although its effect on charge behaviours (namely, charge separation, migration and recombination) is not unitary and requires elaborate control[156,158,159,189]. Doping metals or non-metals is another strategy to tune electronic structures and optical properties of inorganic-semiconductor-based catalysts. Doping can introduce impurity levels, with the dopants having an important role in suppressing charge recombination[20,44,46,190]. In addition, loading cocatalysts such as metal nanoparticles onto semiconductors can extend charge lifetime and provide more active sites. The optical absorption of cocatalysts does not necessarily contribute to CO_2 reduction, which needs further clarification[20,42,72,91]. Moreover, structural and morphological control of catalysts allows adequate exposure of active sites with short charge transfer paths towards catalyst surface[21,39,47,51,70,138,191]. From this perspective, porous materials,

low-dimensional materials and molecular catalysts are preferred. Enhancing the basicity of catalyst surface is also a promising strategy because CO_2 can perform as an electron acceptor to be activated when the electrophilic carbon atom interacts with Lewis basic sites[78,192]. The functions of a catalyst should be synchronized in time and space to have appropriate overall dynamics. Alternatively, combining multiple components as a composite catalyst may make it easier to meet the complicated requirements of efficient photocatalytic CO_2 reduction. Combining two or more semiconductors to form p–n junction or *Z*-scheme promotes separation of charge carriers[20–22]. In addition, the role of light harvesting can be separated from supplying catalytically active sites given efficient interfacial charge transfer[37]. Interestingly, biotic species such as bacteria can be coupled with abiotic ones with electrons and protons (or H_2) transferred across interface, boosting photocatalytic CO_2 reduction[89,91,92].

The second approach to enhance energy conversion efficiency is to optimize reactor and operation conditions. An ideal reactor should ensure efficient mass, photon and heat transfers, which can be improved by adjusting its shape, size and material[8,170]. The placement of solid catalyst, as a slurry, fixed bed or film coated on a substrate, is another essential factor[18]. A rational design of substrates that allows sufficient exposure to light and reactants can significantly increase energy conversion efficiency for a wide range of catalysts[105,133,134]. Moreover, as different catalysts have different optimal reaction conditions to achieve their highest CO_2 reduction efficiency, selecting an appropriate reductant and solvent and tuning the feed ratio, pressure, catalyst dosage and reaction time show a great promise to further enhance energy conversion efficiency.

The development of thermo-photo synergetic catalytic processes has emerged as a promising approach to address the low efficiency of photocatalysis and reduce the large energy consumption of thermal catalysis[18,74,105,158,191]. Thermal energy is either in situ generated via photothermal effect or supplied with external heat source, which promotes photocatalysis through enhancing the kinetic driving force of reactants, tuning redox potentials, facilitating charge carrier migration, accelerating mass transfer, promoting reactant dissociation or adjusting catalyst structure[18,74,105,180].

Low product selectivity

Low product selectivity is another major limitation of photocatalytic CO_2 reduction, which is caused by the complex multi-electron photoreduction reactions towards various carbon-containing substances and competitive H_2 evolution reaction in the presence of proton source. Low product selectivity imposes burden on downstream utilization as separation and purification of products are required. The possible methods to address this issue are as follows.

First, the reaction pathway for every catalytic system should be clarified to determine the best route to direct the reaction towards the desirable product and terminate its further conversion[16,149]. In-depth understanding on reaction pathway at the molecular level can be developed via in situ characterization techniques. However, the contribution of theoretical calculations to mechanistic understanding is limited because they cannot rigorously model real photocatalytic CO_2 reduction systems.

Product selectivity can be tuned by choosing catalysts with appropriate energy band positions. Only thermodynamically favoured CO_2 reduction reactions with redox potentials more positive than the CBM of the catalyst can proceed. Other effective strategies for selectivity control include adjusting energy band positions of a certain catalyst via doping[190,193,194], size tuning (inducing quantum size effect)[195] and defect engineering[74,105].

Furthermore, orienting surface reactions is an important approach to regulate product selectivity, owing to the high dependency of product selectivity on the destiny of surface species, namely, either desorption or further conversion[18,196]. Surface reactions can be oriented by tuning the catalyst surface (for example, elaborately designing the surface structure of nanosized catalysts[47,150,186] and the chemical structure of molecular catalysts[64,65]). In addition, cocatalyst loading[73], crystal facet engineering[138,197], surface layer coating[198] and particle size optimization[42] of solid catalysts might help to control product selectivity. Surface reactions can also be oriented by adjusting reaction medium and condition. For example, if one product shows a high solubility in reaction medium under the operation condition,

Box 1

Limitations and optimizations of photocatalytic CO_2 reduction

The two main limitations of photocatalytic CO_2 reduction are the low solar-to-chemical energy conversion efficiency and low product selectivity.

Low energy conversion efficiency

Causes

- Limited utilization of solar energy
- Difficult activation of CO_2
- Sluggish kinetics of multiple proton-coupled electron transfers

Optimizations

- Exploiting catalysts with sufficient active sites, wide solar-spectrum absorption and efficient charge separation via:
  - Introducing defects
  - Doping metals or non-metals
  - Loading cocatalysts
  - Tuning structure and morphology
  - Enhancing surface basicity
  - Combining multiple components (biotic and abiotic)
- Optimizing reactor and operation conditions
- Developing thermo-photocatalytic processes

Low product selectivity

Causes

- Complex multi-electron reduction reactions towards various carbon-containing products
- Competitive H_2 evolution reaction

Optimizations

- Clarifying reaction pathway
- Choosing catalysts with appropriate energy band positions
- Orienting surface reactions via
  - Tuning catalyst surface
  - Adjusting reaction medium and condition

Glossary

Conduction band minimum
(CBM). The bottom of the lowest range of vacant electronic states.

de Broglie wavelengths
The wavelength manifested in all objects in quantum mechanics that determines the probability density of finding the object at a given point of the configuration space.

Heterogeneous process
The process in which the components are in multiple phases.

Homogeneous process
The process in which all components are in the same phase.

Hot charge carriers
The high-energy non-equilibrium electrons and holes resulting from the decay of plasmonic excitation.

Localized surface plasmon resonance effect
The coherent collective oscillation of conduction band electrons in metal nanoparticles excited by the electromagnetic radiation of incident light.

Scherrer equation
The formula that relates the size of sub-micrometre crystallites in a solid to the broadening of a peak in an X-ray diffraction pattern.

Semiconductor energy band gap
The energy difference between the valence band maximum and the conduction band minimum of a semiconductor.

Thermal catalysis
The process of accelerating a chemical reaction with a catalyst and driven by thermal energy.

Turnover frequency
(TOF). The turnover number per unit time.

Turnover number
(TON). The number of catalytic cycles (here, CO_2 molecules converted) per active site in a certain time.

Valence band maximum
(VBM). The top of the highest range of electronic states that are occupied by electrons at absolute zero temperature.

it can easily desorb from the catalyst surface without further conversion to higher-reduction-state products, leading to its high selectivity. However, in a closed photocatalytic system, the continuous accumulation of a product might result in its further conversion or the backward reaction.

Outlook

Photocatalytic CO_2 reduction is a sustainable strategy that utilizes renewable solar energy to produce high-value chemicals and fuels. The number of publications in this emerging field has markedly increased over recent years and is ever growing. Numerous inspiring progresses have been made in catalyst exploitation, reactor design, process optimization and mechanism exploration, leading to significant improvement of photocatalytic performance. Nevertheless, photocatalytic CO_2 reduction is still far from practical application mainly owing to its uncompetitive activity and selectivity. Here eight directions for boosting the development of this promising field are outlined.

First, existing information of the kinetics of various steps in a photocatalytic CO_2 reduction process, active sites and reaction intermediates is deficient, causing a black box of reaction mechanism. However, a thorough and deep mechanistic understanding is necessary for designing efficient catalysts and catalytic systems. To acquire solid information, in situ irradiated characterizations at high spatial, temporal and spectral resolutions should be developed[138,141,142,145]. In addition, several papers claimed that DFT calculations show or demonstrate their reaction mechanisms, which are not true. Current computational methods cannot rigorously model complex photocatalytic CO_2 reduction systems and energy surfaces in excited states. There is still a long way to go to find a reliable computational method to elucidate catalytic mechanisms. Otherwise, calculation results just serve as a supplementary reference of experimental results.

Second, catalyst design is the core of promoting photocatalytic performance. An ideal catalyst should demonstrate high efficiency, desirable selectivity, excellent stability and recyclability, low cost and environmental friendliness. To optimize catalytic efficiency, wide solar-spectrum absorption, effective charge separation and sufficient active sites must be ensured. To acquire desirable selectivity, the energy band positions and surface structure of catalysts should be elaborately designed. To achieve excellent stability and recyclability, the catalyst should have a good resistance to photocorrosion and all involved chemical substances including reactants, intermediates and products. The economic viability and environmental impacts should be comprehensively evaluated via systematic techno-economic analysis and life cycle assessment. More strategies of optimizing catalysts can be developed on top of the present defect engineering, doping, cocatalyst modification, size regulation, structural and morphological control, surface basicity enhancement and heterostructure fabrication. Porous materials, low-dimensional materials and molecular catalysts show great promise to realize high photocatalytic performance for CO_2 reduction, owing to efficient mass and charge transfers and their regulatable structures. In addition, the application of biological species such as bacteria and enzymes in photocatalytic CO_2 reduction that exhibited great product selectivities[85–87,89,91,92,99] deserves more research attention.

Following the last perspective on experimental exploration of efficient catalysts, advanced first-principles computation and machine learning techniques can assist the screening of candidate materials for photocatalytic CO_2 reduction, owing to recent advances in available computational power and computational methods[155,199]. For example, 52 materials stood out from 68,860 candidates after screening with their synthesizability, visible-light absorption, compatibility of the electronic structure with CO_2 reduction and corrosion resistance[199]. Nevertheless, a large computational data set of material properties is required for facilitating further applications of data-driven techniques. The utilization of big data and machine learning augmented by robotic automation based on the existing knowledge of CO_2 photocatalysis[7,200,201] may pave the way for photocatalyst development.

Despite wide investigation of heterogeneous photocatalytic CO_2 reduction processes, studies in homogeneous photocatalytic CO_2 reduction are still in infancy. The use of molecular catalysts in homogeneous photocatalytic CO_2 reduction is a promising approach because of the easy and ready fine-tuning of ligand structures via controlling steric and electronic effects and their adequate exposure to CO_2, which may lead to highly efficient and selective processes[64,65,102,202]. Future research may be focused on the exploitation of cheap and earth-abundant metal complex catalysts, simplification or automation of catalyst synthesis procedure, improvement of other system components including photosensitizer, electron donor and solvent, and scale-up of current millilitre-level reactors.

Photocatalytic CO_2 reduction can be promoted by introducing another energy source such as thermal, electric, magnetic, ultrasonic,

microwave or mechanical energy, for efficient synergetic catalytic processes[18]. Among these synergetic processes, photoelectrocatalytic CO_2 reduction has been widely studied[17,159,203–205], and thermo-photo catalytic CO_2 reduction is the most attractive because thermal energy can be supplied by the photothermal effect. The photothermal effect can be induced either locally by the catalyst itself[191,206,207] or globally with a solar furnace[185], eliminating the burden on energy consumption. Here, the thermal energy mainly enhances the kinetic driving force of reactants[74,105]. Thermo-photo catalysis perfectly suits gas-phase reactions conducted in flow reactors such as CO_2 hydrogenation[74,158,191] and CO_2 reforming of CH_4 (refs. 105,180,181) as parabolic trough solar concentrators are commercially available.

More effort should be made in the utilization of low-concentration CO_2 feedstock with potential interfering species, for practical application. Currently, 1 atm or even pressurized high-purity CO_2 is used as feedstock. To narrow the gap between laboratorial investigation and practical application, photocatalytic tests with CO_2 concentrations down to the ppm level in the presence of other gases such as O_2, N_2 and SO_2 are expected. The entire catalytic system including catalyst, reductant, reactor and operation conditions should be optimized to attain satisfying performance of converting low-concentration CO_2 into desirable products.

Selective production of multicarbon substances remains a great challenge. Most multicarbon substances demonstrate higher market prices and more versatile uses than those of C1 chemicals (Table 1), which offers strong driving force for improving multicarbon product selectivity. The complicated and sluggish kinetics of converting CO_2 into multicarbon substances and the lack of catalytic activity towards C–C coupling are two main barriers[10,196,208]. It is believed that every factor that benefits the accumulation of charge carriers and protons, such as high photon flux and cocatalyst modification, favours the formation of multicarbon products[10]. Furthermore, the catalyst should keep a balance between its abilities for hydrogenation and C–C coupling, which may reference to those applied in Fischer–Tropsch synthesis.

Finally, it is highly desirable to realize the transition from laboratory to practical and scalable applications in the next 10–20 years. This requires a large effort in catalyst optimization, modelling and construction of catalytic reactor and supporting facilities such as CO_2 collector, solar concentrator and product separator, and assessment of economic and environmental benefits. Ultimately, photocatalytic CO_2 reduction will be an effective and sustainable answer to the critical issues related to energy and environment.

Photocatalytic CO_2 reduction is a highly promising method to valourize the anthropogenic CO_2 emissions, having raised a huge amount of research interests in the science community. A thorough understanding of this method, from the physical and chemical principles to the experimentation techniques and data reporting standards, is crucial for obtaining reliable and useful conclusions and driving the ongoing progress in our shared area. This Primer is expected to help overcome the current issues with data reproducibility and deposition and facilitate the laboratory-to-industry transition through combining the elaborate design of catalytic systems and deep exploration of reaction mechanisms. We believe that, with greater interactions and collaborations among experimental scientists, theorists, engineers and regulatory agencies, more exciting discoveries are ahead.

Published online: 10 August 2023

References

1. Wang, L. et al. Surface strategies for catalytic CO_2 reduction: from two-dimensional materials to nanoclusters to single atoms. *Chem. Soc. Rev.* **48**, 5310–5349 (2019). **This article summarizes the surface modification strategies for low-dimensional catalysts applied in heterogeneous photocatalytic CO_2 reduction.**
2. Friedlingstein, P. et al. Global carbon budget 2022. *Earth Syst. Sci. Data* **14**, 4811–4900 (2022).
3. Al-Ghussain, L. Global warming: review on driving forces and mitigation. *Environ. Prog. Sustain. Energy* **38**, 13–21 (2019).
4. Armstrong McKay, D. I. et al. Exceeding 1.5 °C global warming could trigger multiple climate tipping points. *Science* **377**, eabn7950 (2022).
5. Li, X., Yu, J., Jaroniec, M. & Chen, X. Cocatalysts for selective photoreduction of CO_2 into solar fuels. *Chem. Rev.* **119**, 3962–4179 (2019). **This is a comprehensive review regarding the roles, designs, modifications and applications of cocatalysts for photocatalytic CO_2 reduction.**
6. Hu, Y. H. & Ruckenstein, E. Comment on "Dry reforming of methane by stable Ni–Mo nanocatalysts on single-crystalline MgO". *Science* **368**, eabb5459 (2020).
7. Ozin, G. Accelerated optochemical engineering solutions to CO_2 photocatalysis for a sustainable future. *Matter* **5**, 2594–2614 (2022).
8. Tountas, A. A. et al. Towards solar methanol: past, present, and future. *Adv. Sci.* **6**, 1801903 (2019).
9. Fang, S. et al. Turning dead leaves into an active multifunctional material as evaporator, photocatalyst, and bioplastic. *Nat. Commun.* **14**, 1203 (2023).
10. Albero, J., Peng, Y. & García, H. Photocatalytic CO_2 reduction to C2+ products. *ACS Catal.* **10**, 5734–5749 (2020).
11. Wei, J., Yao, R., Han, Y., Ge, Q. & Sun, J. Towards the development of the emerging process of CO_2 heterogenous hydrogenation into high-value unsaturated heavy hydrocarbons. *Chem. Soc. Rev.* **50**, 10764–10805 (2021).
12. Li, M., Sun, Z. & Hu, Y. H. Catalysts for CO_2 reforming of CH_4: a review. *J. Mater. Chem. A* **9**, 12495–12520 (2021).
13. Wagner, A., Sahm, C. D. & Reisner, E. Towards molecular understanding of local chemical environment effects in electro- and photocatalytic CO_2 reduction. *Nat. Catal.* **3**, 775–786 (2020).
14. Birdja, Y. Y. et al. Advances and challenges in understanding the electrocatalytic conversion of carbon dioxide to fuels. *Nat. Energy* **4**, 732–745 (2019).
15. Wang, C., Sun, Z., Zheng, Y. & Hu, Y. H. Recent progress in visible light photocatalytic conversion of carbon dioxide. *J. Mater. Chem. A* **7**, 865–887 (2019).
16. Chang, X., Wang, T. & Gong, J. CO_2 photo-reduction: insights into CO_2 activation and reaction on surfaces of photocatalysts. *Energy Environ. Sci.* **9**, 2177–2196 (2016).
17. Inoue, T., Fujishima, A., Konishi, S. & Honda, K. Photoelectrocatalytic reduction of carbon dioxide in aqueous suspensions of semiconductor powders. *Nature* **277**, 637–638 (1979). **To our knowledge, this is the first known report on heterogeneous photocatalytic CO_2 reduction.**
18. Fang, S. & Hu, Y. H. Thermo-photo catalysis: a whole greater than the sum of its parts. *Chem. Soc. Rev.* **51**, 3609–3647 (2022).
19. Li, K., Peng, B. & Peng, T. Recent advances in heterogeneous photocatalytic CO_2 conversion to solar fuels. *ACS Catal.* **6**, 7485–7527 (2016).
20. Wang, Q. et al. Molecularly engineered photocatalyst sheet for scalable solar formate production from carbon dioxide and water. *Nat. Energy* **5**, 703–710 (2020). **This is a representative work of heterogenizing a molecular catalyst on a light-absorbing semiconductor sheet.**
21. Wang, S. et al. Porous hypercrosslinked polymer-TiO_2-graphene composite photocatalysts for visible-light-driven CO_2 conversion. *Nat. Commun.* **10**, 676 (2019).
22. Wang, Y. et al. Direct and indirect Z-scheme heterostructure-coupled photosystem enabling cooperation of CO_2 reduction and H_2O oxidation. *Nat. Commun.* **11**, 3043 (2020).
23. Yan, T. et al. How to make an efficient gas-phase heterogeneous CO_2 hydrogenation photocatalyst. *Energy Environ. Sci.* **13**, 3054–3063 (2020).
24. Shangguan, W. et al. Molecular-level insight into photocatalytic CO_2 reduction with H_2O over Au nanoparticles by interband transitions. *Nat. Commun.* **13**, 3894 (2022).
25. Li, Y. et al. Boosting thermo-photocatalytic CO_2 conversion activity by using photosynthesis-inspired electron–proton-transfer mediators. *Nat. Commun.* **12**, 123 (2021).
26. Zhang, X. et al. Product selectivity in plasmonic photocatalysis for carbon dioxide hydrogenation. *Nat. Commun.* **8**, 14542 (2017).
27. Devasia, D., Wilson, A. J., Heo, J., Mohan, V. & Jain, P. K. A rich catalog of C–C bonded species formed in CO_2 reduction on a plasmonic photocatalyst. *Nat. Commun.* **12**, 2612 (2021).
28. Zhan, C. et al. Plasmon-mediated chemical reactions. *Nat. Rev. Methods Primers* **3**, 12 (2023).
29. Zhan, C. et al. Disentangling charge carrier from photothermal effects in plasmonic metal nanostructures. *Nat. Commun.* **10**, 2671 (2019).
30. Kuramochi, Y., Ishitani, O. & Ishida, H. Reaction mechanisms of catalytic photochemical CO_2 reduction using Re(I) and Ru(II) complexes. *Coord. Chem. Rev.* **373**, 333–356 (2018).
31. Yamazaki, Y., Takeda, H. & Ishitani, O. Photocatalytic reduction of CO_2 using metal complexes. *J. Photochem. Photobiol. C* **25**, 106–137 (2015). **This article provides an overview on homogeneous photocatalytic CO_2 reduction processes over metal complexes.**

32. Perazio, A., Lowe, G., Gobetto, R., Bonin, J. & Robert, M. Light-driven catalytic conversion of CO_2 with heterogenized molecular catalysts based on fourth period transition metals. *Coord. Chem. Rev.* **443**, 214018 (2021).
33. Sun, W. et al. Heterogeneous reduction of carbon dioxide by hydride-terminated silicon nanocrystals. *Nat. Commun.* **7**, 12553 (2016).
34. Chen, G. et al. Alumina-supported CoFe alloy catalysts derived from layered-double-hydroxide nanosheets for efficient photothermal CO_2 hydrogenation to hydrocarbons. *Adv. Mater.* **30**, 1704663 (2018).
35. Hao, Y.-C. et al. Metal–organic framework membranes with single-atomic centers for photocatalytic CO_2 and O_2 reduction. *Nat. Commun.* **12**, 2682 (2021).
36. Niu, K. et al. A spongy nickel-organic CO_2 reduction photocatalyst for nearly 100% selective CO production. *Sci. Adv.* **3**, e1700921 (2017).
37. Jiang, Z. et al. Filling metal–organic framework mesopores with TiO_2 for CO_2 photoreduction. *Nature* **586**, 549–554 (2020).
This work develops an efficient heterostructure photocatalyst by growing the light-absorbing TiO_2 inside the catalytically active MOF backbone.
38. Lan, G. et al. Biomimetic active sites on monolayered metal–organic frameworks for artificial photosynthesis. *Nat. Catal.* **5**, 1006–1018 (2022).
39. Li, H., Cheng, C., Yang, Z. & Wei, J. Encapsulated CdSe/CdS nanorods in double-shelled porous nanocomposites for efficient photocatalytic CO_2 reduction. *Nat. Commun.* **13**, 6466 (2022).
40. Zhou, J. et al. Linking oxidative and reductive clusters to prepare crystalline porous catalysts for photocatalytic CO_2 reduction with H_2O. *Nat. Commun.* **13**, 4681 (2022).
41. Zhong, W. et al. A covalent organic framework bearing single Ni sites as a synergistic photocatalyst for selective photoreduction of CO_2 to CO. *J. Am. Chem. Soc.* **141**, 7615–7621 (2019).
This report presents a COF catalyst bearing single Ni sites for photocatalytic CO_2 reduction to CO.
42. Dong, C. et al. Size-dependent activity and selectivity of carbon dioxide photocatalytic reduction over platinum nanoparticles. *Nat. Commun.* **9**, 1252 (2018).
43. Wan, L. et al. Cu_2O nanocubes with mixed oxidation-state facets for (photo)catalytic hydrogenation of carbon dioxide. *Nat. Catal.* **2**, 889–898 (2019).
44. Sayed, M. et al. Sustained CO_2-photoreduction activity and high selectivity over Mn, C-codoped ZnO core-triple shell hollow spheres. *Nat. Commun.* **12**, 4936 (2021).
45. Yan, T. et al. Polymorph selection towards photocatalytic gaseous CO_2 hydrogenation. *Nat. Commun.* **10**, 2521 (2019).
46. Shown, I. et al. Carbon-doped SnS_2 nanostructure as a high-efficiency solar fuel catalyst under visible light. *Nat. Commun.* **9**, 169 (2018).
47. Li, X. et al. Selective visible-light-driven photocatalytic CO_2 reduction to CH_4 mediated by atomically thin $CuIn_5S_8$ layers. *Nat. Energy* **4**, 690–699 (2019).
This work explores a representative 2D defect-rich photocatalyst for photocatalytic CO_2 reduction.
48. Kuehnel, M. F., Orchard, K. L., Dalle, K. E. & Reisner, E. Selective photocatalytic CO_2 reduction in water through anchoring of a molecular Ni catalyst on CdS nanocrystals. *J. Am. Chem. Soc.* **139**, 7217–7223 (2017).
49. Feng, X. et al. Unlocking bimetallic active sites via a desalination strategy for photocatalytic reduction of atmospheric carbon dioxide. *Nat. Commun.* **13**, 2146 (2022).
50. Shi, Y. et al. Van der Waals gap-rich BiOCl atomic layers realizing efficient, pure-water CO_2-to-CO photocatalysis. *Nat. Commun.* **12**, 5923 (2021).
51. Di, J. et al. Isolated single atom cobalt in Bi_3O_4Br atomic layers to trigger efficient CO_2 photoreduction. *Nat. Commun.* **10**, 2840 (2019).
52. Li, M. M. J. et al. CO_2 hydrogenation to methanol over catalysts derived from single cationic layer CuZnGa LDH precursors. *ACS Catal.* **8**, 4390–4401 (2018).
53. Huang, P. et al. Selective CO_2 reduction catalyzed by single cobalt sites on carbon nitride under visible-light irradiation. *J. Am. Chem. Soc.* **140**, 16042–16047 (2018).
54. Bie, C., Zhu, B., Xu, F., Zhang, L. & Yu, J. In situ grown monolayer N-doped graphene on CdS hollow spheres with seamless contact for photocatalytic CO_2 reduction. *Adv. Mater.* **31**, 1902868 (2019).
55. Zhu, X. et al. In-situ hydroxyl modification of monolayer black phosphorus for stable photocatalytic carbon dioxide conversion. *Appl. Catal. B* **269**, 118760 (2020).
56. Zhao, F. et al. Two-dimensional gersiloxenes with tunable bandgap for photocatalytic H_2 evolution and CO_2 photoreduction to CO. *Nat. Commun.* **11**, 1443 (2020).
57. Roy, S. & Reisner, E. Visible-light-driven CO_2 reduction by mesoporous carbon nitride modified with polymeric cobalt phthalocyanine. *Angew. Chem. Int. Ed.* **58**, 12180–12184 (2019).
58. Wei, Y. et al. Highly efficient photocatalytic reduction of CO_2 to CO by in situ formation of a hybrid catalytic system based on molecular iron quaterpyridine covalently linked to carbon nitride. *Angew. Chem. Int. Ed.* **61**, e202116832 (2022).
59. Ma, B. et al. Hybridization of molecular and graphene materials for CO_2 photocatalytic reduction with selectivity control. *J. Am. Chem. Soc.* **143**, 8414–8425 (2021).
60. Stock, N. & Biswas, S. Synthesis of metal–organic frameworks (MOFs): routes to various MOF topologies, morphologies, and composites. *Chem. Rev.* **112**, 933–969 (2012).
61. Li, Y., Chen, W., Xing, G., Jiang, D. & Chen, L. New synthetic strategies toward covalent organic frameworks. *Chem. Soc. Rev.* **49**, 2852–2868 (2020).
62. Wang, J.-W. et al. Facile electron delivery from graphene template to ultrathin metal-organic layers for boosting CO_2 photoreduction. *Nat. Commun.* **12**, 813 (2021).
63. Yuan, H., Cheng, B., Lei, J., Jiang, L. & Han, Z. Promoting photocatalytic CO_2 reduction with a molecular copper purpurin chromophore. *Nat. Commun.* **12**, 1835 (2021).
64. Rao, H., Schmidt, L. C., Bonin, J. & Robert, M. Visible-light-driven methane formation from CO_2 with a molecular iron catalyst. *Nature* **548**, 74–77 (2017).
This is a representative work on homogeneous photocatalytic CO_2 reduction with a low-cost molecular iron catalyst.
65. Guo, Z. et al. Selectivity control of CO versus $HCOO^-$ production in the visible-light-driven catalytic reduction of CO_2 with two cooperative metal sites. *Nat. Catal.* **2**, 801–808 (2019).
This work develops a binuclear molecular cobalt catalyst for homogeneous photocatalytic CO_2 reduction towards formate.
66. Wu, Y., Li, S., Chen, Y., He, W. & Guo, Z. Recent advances in noble metal complex based photodynamic therapy. *Chem. Sci.* **13**, 5085–5106 (2022).
67. Warnan, J. & Reisner, E. Synthetic organic design for solar fuel systems. *Angew. Chem. Int. Ed.* **59**, 17344–17354 (2020).
68. Hutton, G. A. M., Martindale, B. C. M. & Reisner, E. Carbon dots as photosensitisers for solar-driven catalysis. *Chem. Soc. Rev.* **46**, 6111–6123 (2017).
69. Lim, S. Y., Shen, W. & Gao, Z. Carbon quantum dots and their applications. *Chem. Soc. Rev.* **44**, 362–381 (2015).
70. Ma, Y. et al. Selective photocatalytic CO_2 reduction in aerobic environment by microporous pd-porphyrin-based polymers coated hollow TiO_2. *Nat. Commun.* **13**, 1400 (2022).
71. Wang, S. et al. Intermolecular cascaded π-conjugation channels for electron delivery powering CO_2 photoreduction. *Nat. Commun.* **11**, 1149 (2020).
This work develops a photocatalyst consisting of conjugated polymers for photocatalytic CO_2 reduction to CO.
72. Cao, Y. et al. Modulating electron density of vacancy site by single Au atom for effective CO_2 photoreduction. *Nat. Commun.* **12**, 1675 (2021).
73. Verma, P. et al. Charge-transfer regulated visible light driven photocatalytic H_2 production and CO_2 reduction in tetrathiafulvalene based coordination polymer gel. *Nat. Commun.* **12**, 7313 (2021).
74. Wang, C., Fang, S., Xie, S., Zheng, Y. & Hu, Y. H. Thermo-photo catalytic CO_2 hydrogenation over Ru/TiO_2. *J. Mater. Chem. A* **8**, 7390–7394 (2020).
75. Kang, Q. et al. Photocatalytic reduction of carbon dioxide by hydrous hydrazine over Au–Cu alloy nanoparticles supported on $SrTiO_3/TiO_2$ coaxial nanotube arrays. *Angew. Chem. Int. Ed.* **54**, 841–845 (2015).
76. Zhang, X. et al. Photocatalytic conversion of diluted CO_2 into light hydrocarbons using periodically modulated multiwalled nanotube arrays. *Angew. Chem. Int. Ed.* **51**, 12732–12735 (2012).
77. Jiang, M., Gao, Y., Wang, Z. & Ding, Z. Photocatalytic CO_2 reduction promoted by a $CuCo_2O_4$ cocatalyst with homogeneous and heterogeneous light harvesters. *Appl. Catal. B* **198**, 180–188 (2016).
78. Xie, S., Wang, Y., Zhang, Q., Deng, W. & Wang, Y. MgO- and Pt-promoted TiO_2 as an efficient photocatalyst for the preferential reduction of carbon dioxide in the presence of water. *ACS Catal.* **4**, 3644–3653 (2014).
This work compares the solid–vapour and solid–liquid–gas reaction modes for photocatalytic reduction of CO_2 with H_2O.
79. Lu, K.-Q. et al. Rationally designed transition metal hydroxide nanosheet arrays on graphene for artificial CO_2 reduction. *Nat. Commun.* **11**, 5181 (2020).
80. Zhou, Y. et al. Regulating photocatalytic CO_2 reduction selectivity via steering cascade multi-step charge transfer pathways in $1T/2H\text{-}WS_2/TiO_2$ heterojunctions. *Chem. Eng. J.* **447**, 137485 (2022).
81. Cao, S., Shen, B., Tong, T., Fu, J. & Yu, J. 2D/2D heterojunction of ultrathin MXene/Bi_2WO_6 nanosheets for improved photocatalytic CO_2 reduction. *Adv. Funct. Mater.* **28**, 1800136 (2018).
82. Di, J. et al. Cobalt nitride as a novel cocatalyst to boost photocatalytic CO_2 reduction. *Nano Energy* **79**, 105429 (2021).
83. Tu, W. et al. An in situ simultaneous reduction-hydrolysis technique for fabrication of TiO_2-graphene 2D sandwich-like hybrid nanosheets: graphene-promoted selectivity of photocatalytic-driven hydrogenation and coupling of CO_2 into methane and ethane. *Adv. Funct. Mater.* **23**, 1743–1749 (2013).
84. Badiani, V. M. et al. Engineering electro- and photocatalytic carbon materials for CO_2 reduction by formate dehydrogenase. *J. Am. Chem. Soc.* **144**, 14207–14216 (2022).
85. Miller, M. et al. Interfacing formate dehydrogenase with metal oxides for the reversible electrocatalysis and solar-driven reduction of carbon dioxide. *Angew. Chem. Int. Ed.* **58**, 4601–4605 (2019).
86. Woolerton, T. W., Sheard, S., Pierce, E., Ragsdale, S. W. & Armstrong, F. A. CO_2 photoreduction at enzyme-modified metal oxide nanoparticles. *Energy Environ. Sci.* **4**, 2393–2399 (2011).
87. Liu, X. et al. A genetically encoded photosensitizer protein facilitates the rational design of a miniature photocatalytic CO_2-reducing enzyme. *Nat. Chem.* **10**, 1201–1206 (2018).
88. Kang, F. et al. Rational design of a miniature photocatalytic CO_2-reducing enzyme. *ACS Catal.* **11**, 5628–5635 (2021).
89. Wang, X. et al. Photocatalyst-mineralized biofilms as living bio-abiotic interfaces for single enzyme to whole-cell photocatalytic applications. *Sci. Adv.* **8**, eabm7665 (2022).
90. Ye, J. et al. Solar-driven methanogenesis with ultrahigh selectivity by turning down H_2 production at biotic–abiotic interface. *Nat. Commun.* **13**, 6612 (2022).
91. Wang, Q., Kalathil, S., Pornrungroj, C., Sahm, C. D. & Reisner, E. Bacteria–photocatalyst sheet for sustainable carbon dioxide utilization. *Nat. Catal.* **5**, 633–641 (2022).

92. Sakimoto, K. K., Wong, A. B. & Yang, P. Self-photosensitization of nonphotosynthetic bacteria for solar-to-chemical production. *Science* **351**, 74–77 (2016).
This work develops a biological–inorganic hybrid with non-photosynthetic bacteria and light-absorbing CdS nanoparticles.
93. Lam, E. & Reisner, E. A TiO_2-co(terpyridine)$_2$ photocatalyst for the selective oxidation of cellulose to formate coupled to the reduction of CO_2 to syngas. *Angew. Chem. Int. Ed.* **60**, 23306–23312 (2021).
94. Bi, Q.-Q. et al. Selective photocatalytic CO_2 reduction in water by electrostatic assembly of CdS nanocrystals with a dinuclear cobalt catalyst. *ACS Catal.* **8**, 11815–11821 (2018).
95. Liu, L., Zhao, H., Andino, J. M. & Li, Y. Photocatalytic CO_2 reduction with H_2O on TiO_2 nanocrystals: comparison of anatase, rutile, and brookite polymorphs and exploration of surface chemistry. *ACS Catal.* **2**, 1817–1828 (2012).
96. Wang, K. et al. Unravelling the C–C coupling in CO_2 photocatalytic reduction with H_2O on Au/TiO_{2-x}: combination of plasmonic excitation and oxygen vacancy. *Appl. Catal. B* **292**, 120147 (2021).
97. Kornienko, N., Zhang, J. Z., Sakimoto, K. K., Yang, P. & Reisner, E. Interfacing nature's catalytic machinery with synthetic materials for semi-artificial photosynthesis. *Nat. Nanotechnol.* **13**, 890–899 (2018).
98. Fang, X., Kalathil, S. & Reisner, E. Semi-biological approaches to solar-to-chemical conversion. *Chem. Soc. Rev.* **49**, 4926–4952 (2020).
99. Zhang, H. et al. Bacteria photosensitized by intracellular gold nanoclusters for solar fuel production. *Nat. Nanotechnol.* **13**, 900–905 (2018).
100. Dalle, K. E. et al. Electro- and solar-driven fuel synthesis with first row transition metal complexes. *Chem. Rev.* **119**, 2752–2875 (2019).
101. Guo, Z. et al. Highly efficient and selective photocatalytic CO_2 reduction by iron and cobalt quaterpyridine complexes. *J. Am. Chem. Soc.* **138**, 9413–9416 (2016).
102. Bonin, J., Robert, M. & Routier, M. Selective and efficient photocatalytic CO_2 reduction to CO using visible light and an iron-based homogeneous catalyst. *J. Am. Chem. Soc.* **136**, 16768–16771 (2014).
103. Cometto, C. et al. A carbon nitride/Fe quaterpyridine catalytic system for photostimulated CO_2-to-CO conversion with visible light. *J. Am. Chem. Soc.* **140**, 7437–7440 (2018).
104. Ran, J., Jaroniec, M. & Qiao, S.-Z. Cocatalysts in semiconductor-based photocatalytic CO_2 reduction: achievements, challenges, and opportunities. *Adv. Mater.* **30**, 1704649 (2018).
105. Han, B., Wei, W., Chang, L., Cheng, P. & Hu, Y. H. Efficient visible light photocatalytic CO_2 reforming of CH_4. *ACS Catal.* **6**, 494–497 (2016).
To our knowledge, this is the first known report on photocatalytic CO_2 reduction by CH_4 owing to the synergetic effects of photo and thermal energies.
106. Cancelliere, A. M. et al. Efficient trinuclear Ru(II)–Re(I) supramolecular photocatalysts for CO_2 reduction based on a new tris-chelating bridging ligand built around a central aromatic ring. *Chem. Sci.* **11**, 1556–1563 (2020).
107. Hargreaves, J. S. J. Some considerations related to the use of the Scherrer equation in powder X-ray diffraction as applied to heterogeneous catalysts. *Catal. Struct. React.* **2**, 33–37 (2016).
108. Inkson, B. J. in *Materials Characterization Using Nondestructive Evaluation (NDE) Methods* (eds Hübschen, G., Altpeter, I., Tschuncky, R., & Herrmann, H.-G.) 17–43 (Woodhead Publishing, 2016).
109. Carter, C. B. & Williams, D. B. *Transmission Electron Microscopy: Diffraction, Imaging, and Spectrometry* (Springer, 2016).
110. Fang, S. & Hu, Y. H. Open the door to the atomic world by single-molecule atomic force microscopy. *Matter* **4**, 1189–1223 (2021).
111. Zhang, L., Ran, J., Qiao, S.-Z. & Jaroniec, M. Characterization of semiconductor photocatalysts. *Chem. Soc. Rev.* **48**, 5184–5206 (2019).
112. Zhang, Y., Xia, B., Ran, J., Davey, K. & Qiao, S. Z. Atomic-level reactive sites for semiconductor-based photocatalytic CO_2 reduction. *Adv. Energy Mater.* **10**, 1903879 (2020).
113. Wertz, J. *Electron Spin Resonance: Elementary Theory and Practical Applications* (Springer Science & Business Media, 2012).
114. Van der Heide, P. *X-ray Photoelectron Spectroscopy: An Introduction to Principles and Practices* (John Wiley & Sons, 2011).
115. de Groot, F. High-resolution X-ray emission and X-ray absorption spectroscopy. *Chem. Rev.* **101**, 1779–1808 (2001).
116. Lambert, J. B., Mazzola, E. P. & Ridge, C. D. *Nuclear Magnetic Resonance Spectroscopy: An Introduction to Principles, Applications, and Experimental Methods* (John Wiley & Sons, 2019).
117. Larkin, P. *Infrared and Raman Spectroscopy: Principles and Spectral Interpretation* (Elsevier, 2017).
118. Makuła, P., Pacia, M. & Macyk, W. How to correctly determine the band gap energy of modified semiconductor photocatalysts based on UV–Vis spectra. *J. Phys. Chem. Lett.* **9**, 6814–6817 (2018).
119. Miao, T. J. & Tang, J. Characterization of charge carrier behavior in photocatalysis using transient absorption spectroscopy. *J. Chem. Phys.* **152**, 194201 (2020).
120. Wang, S. et al. Electrochemical impedance spectroscopy. *Nat. Rev. Methods Primers* **1**, 41 (2021).
121. Jones, W. E. Jr. & Fox, M. A. Determination of excited-state redox potentials by phase-modulated voltammetry. *J. Phys. Chem.* **98**, 5095–5099 (1994).
122. Zhang, Y., Petersen, J. L. & Milsmann, C. A luminescent zirconium(IV) complex as a molecular photosensitizer for visible light photoredox catalysis. *J. Am. Chem. Soc.* **138**, 13115–13118 (2016).
123. Kahn, A. Fermi level, work function and vacuum level. *Mater. Horiz.* **3**, 7–10 (2016).
124. Mohan, A. et al. Hybrid photo- and thermal catalyst system for continuous CO_2 reduction. *ACS Appl. Mater. Interfaces* **12**, 33613–33620 (2020).
125. Hurtado, L. et al. Solar CO_2 hydrogenation by photocatalytic foams. *Chem. Eng. J.* **435**, 134864 (2022).
126. Han, B. & Hu, Y. H. Highly efficient temperature-induced visible light photocatalytic hydrogen production from water. *J. Phys. Chem. C* **119**, 18927–18934 (2015).
127. Chen, S. et al. Thin-water-film-enhanced TiO_2-based catalyst for CO_2 hydrogenation to formic acid. *Chem. Commun.* **58**, 787–790 (2022).
128. Ola, O. & Maroto-Valer, M. M. Review of material design and reactor engineering on TiO_2 photocatalysis for CO_2 reduction. *J. Photochem. Photobiol. C* **24**, 16–42 (2015).
129. Gong, E. et al. Solar fuels: research and development strategies to accelerate photocatalytic CO_2 conversion into hydrocarbon fuels. *Energy Environ. Sci.* **15**, 880–937 (2022).
130. Tahir, M. & Amin, N. S. Photocatalytic CO_2 reduction with H_2O vapors using montmorillonite/TiO_2 supported microchannel monolith photoreactor. *Chem. Eng. J.* **230**, 314–327 (2013).
131. Wu, J. C. S., Lin, H.-M. & Lai, C.-L. Photo reduction of CO_2 to methanol using optical-fiber photoreactor. *Appl. Catal. A* **296**, 194–200 (2005).
132. Nguyen, T.-V. & Wu, J. C. S. Photoreduction of CO_2 in an optical-fiber photoreactor: effects of metals addition and catalyst carrier. *Appl. Catal. A* **335**, 112–120 (2008).
133. Liou, P.-Y. et al. Photocatalytic CO_2 reduction using an internally illuminated monolith photoreactor. *Energy Environ. Sci.* **4**, 1487–1494 (2011).
134. Xiong, Z. et al. Photocatalytic CO_2 reduction over V and W codoped TiO_2 catalyst in an internal-illuminated honeycomb photoreactor under simulated sunlight irradiation. *Appl. Catal. B* **219**, 412–424 (2017).
135. Chatterjee, T., Boutin, E. & Robert, M. Manifesto for the routine use of NMR for the liquid product analysis of aqueous CO_2 reduction: from comprehensive chemical shift data to formaldehyde quantification in water. *Dalton Trans.* **49**, 4257–4265 (2020).
136. Wang, L., Cheng, B., Zhang, L. & Yu, J. In situ irradiated XPS investigation on S-scheme TiO_2@$ZnIn_2S_4$ photocatalyst for efficient photocatalytic CO_2 reduction. *Small* **17**, 2103447 (2021).
137. Collado, L. et al. Unravelling the effect of charge dynamics at the plasmonic metal/semiconductor interface for CO_2 photoreduction. *Nat. Commun.* **9**, 4986 (2018).
138. Wu, Y. A. et al. Facet-dependent active sites of a single Cu_2O particle photocatalyst for CO_2 reduction to methanol. *Nat. Energy* **4**, 957–968 (2019).
This article offers atomic-level understanding of active sites and chemical reaction mechanisms via in situ scanning fluorescence X-ray microscopy–environmental transmission electron microscopy technique.
139. Yan, Z.-H. et al. Photo-generated dinuclear {Eu(II)}$_2$ active sites for selective CO_2 reduction in a photosensitizing metal-organic framework. *Nat. Commun.* **9**, 3353 (2018).
140. Wang, M. et al. CO_2 electrochemical catalytic reduction with a highly active cobalt phthalocyanine. *Nat. Commun.* **10**, 3602 (2019).
141. Abdellah, M. et al. Time-resolved IR spectroscopy reveals a mechanism with TiO_2 as a reversible electron acceptor in a TiO_2–Re catalyst system for CO_2 photoreduction. *J. Am. Chem. Soc.* **139**, 1226–1232 (2017).
142. Hu, Y. et al. Tracking mechanistic pathway of photocatalytic CO_2 reaction at Ni sites using operando, time-resolved spectroscopy. *J. Am. Chem. Soc.* **142**, 5618–5626 (2020).
143. Tan, T. H. et al. Unlocking the potential of the formate pathway in the photo-assisted Sabatier reaction. *Nat. Catal.* **3**, 1034–1043 (2020).
This article provides a mechanistic understanding on photo-activation of adsorbed formate intermediate in photocatalytic CO_2 hydrogenation.
144. Dimitrijevic, N. M., Shkrob, I. A., Gosztola, D. J. & Rajh, T. Dynamics of interfacial charge transfer to formic acid, formaldehyde, and methanol on the surface of TiO_2 nanoparticles and its role in methane production. *J. Phys. Chem. C.* **116**, 878–885 (2012).
145. Lee, J., Sorescu, D. C. & Deng, X. Electron-induced dissociation of CO_2 on TiO_2(110). *J. Am. Chem. Soc.* **133**, 10066–10069 (2011).
146. Verma, R. et al. Nickel-laden dendritic plasmonic colloidosomes of black gold: forced plasmon mediated photocatalytic CO_2 hydrogenation. *ACS Nano* **17**, 4526–4538 (2023).
147. Dhiman, M. et al. Plasmonic colloidosomes of black gold for solar energy harvesting and hotspots directed catalysis for CO_2 to fuel conversion. *Chem. Sci.* **10**, 6594–6603 (2019).
148. Qin, D. et al. Recent advances in two-dimensional nanomaterials for photocatalytic reduction of CO_2: insights into performance, theories and perspective. *J. Mater. Chem. A* **8**, 19156–19195 (2020).
149. Hussain, S., Wang, Y., Guo, L. & He, T. Theoretical insights into the mechanism of photocatalytic reduction of CO_2 over semiconductor catalysts. *J. Photochem. Photobiol. C* **52**, 100538 (2022).
150. Li, J. et al. Self-adaptive dual-metal-site pairs in metal–organic frameworks for selective CO_2 photoreduction to CH_4. *Nat. Catal.* **4**, 719–729 (2021).
This report presents the selective photocatalytic CO_2 reduction to CH_4 over the MOF incorporated with self-adaptive dual-metal-site pairs.
151. Kovačič, Ž., Likozar, B. & Huš, M. Photocatalytic CO_2 reduction: a review of ab initio mechanism, kinetics, and multiscale modeling simulations. *ACS Catal.* **10**, 14984–15007 (2020).
152. Chu, W., Zheng, Q., Prezhdo, O. V. & Zhao, J. CO_2 photoreduction on metal oxide surface is driven by transient capture of hot electrons: ab initio quantum dynamics simulation. *J. Am. Chem. Soc.* **142**, 3214–3221 (2020).

153. Mai, H., Le, T. C., Chen, D., Winkler, D. A. & Caruso, R. A. Machine learning for electrocatalyst and photocatalyst design and discovery. *Chem. Rev.* **122**, 13478–13515 (2022).
154. Cheng, S. et al. Emerging strategies for CO_2 photoreduction to CH_4: from experimental to data-driven design. *Adv. Energy Mater.* **12**, 2200389 (2022).
155. Zhu, Q., Gu, Y., Liang, X., Wang, X. & Ma, J. A machine learning model to predict CO_2 reduction reactivity and products transferred from metal-zeolites. *ACS Catal.* **12**, 12336–12348 (2022).
156. Gao, W. et al. Vacancy-defect modulated pathway of photoreduction of CO_2 on single atomically thin $AgInP_2S_6$ sheets into olefiant gas. *Nat. Commun.* **12**, 4747 (2021).
157. Andrei, V., Wang, Q., Uekert, T., Bhattacharjee, S. & Reisner, E. Solar panel technologies for light-to-chemical conversion. *Acc. Chem. Res.* **55**, 3376–3386 (2022).
158. Wang, L. et al. Black indium oxide a photothermal CO_2 hydrogenation catalyst. *Nat. Commun.* **11**, 2432 (2020).
159. Yu, H. et al. Synergy of ferroelectric polarization and oxygen vacancy to promote CO_2 photoreduction. *Nat. Commun.* **12**, 4594 (2021).
160. Wang, J.-W., Jiang, L., Huang, H.-H., Han, Z. & Ouyang, G. Rapid electron transfer via dynamic coordinative interaction boosts quantum efficiency for photocatalytic CO_2 reduction. *Nat. Commun.* **12**, 4276 (2021).
161. Scott, S. L. A matter of life(time) and death. *ACS Catal.* **8**, 8597–8599 (2018).
162. Masel, R. I. et al. An industrial perspective on catalysts for low-temperature CO_2 electrolysis. *Nat. Nanotechnol.* **16**, 118–128 (2021).
163. Baruch, M. F., Pander, J. E. III, White, J. L. & Bocarsly, A. B. Mechanistic insights into the reduction of CO_2 on tin electrodes using in situ ATR-IR spectroscopy. *ACS Catal.* **5**, 3148–3156 (2015).
164. Kortlever, R., Shen, J., Schouten, K. J. P., Calle-Vallejo, F. & Koper, M. T. M. Catalysts and reaction pathways for the electrochemical reduction of carbon dioxide. *J. Phys. Chem. Lett.* **6**, 4073–4082 (2015).
165. Wang, Y., Chen, E. & Tang, J. Insight on reaction pathways of photocatalytic CO_2 conversion. *ACS Catal.* **12**, 7300–7316 (2022).
166. Yamazaki, Y., Miyaji, M. & Ishitani, O. Utilization of low-concentration CO_2 with molecular catalysts assisted by CO_2-capturing ability of catalysts, additives, or reaction media. *J. Am. Chem. Soc.* **144**, 6640–6660 (2022).
167. Dong, Y. et al. Shining light on CO_2: from materials discovery to photocatalyst, photoreactor and process engineering. *Chem. Soc. Rev.* **49**, 5648–5663 (2020).
168. Schroeder, E. & Christopher, P. Chemical production using light: are sustainable photons cheap enough? *ACS Energy Lett.* **7**, 880–884 (2022).
169. Loh, J. Y. Y., Kherani, N. P. & Ozin, G. A. Persistent CO_2 photocatalysis for solar fuels in the dark. *Nat. Sustain.* **4**, 466–473 (2021).
170. Van Gerven, T., Mul, G., Moulijn, J. & Stankiewicz, A. A review of intensification of photocatalytic processes. *Chem. Eng. Process.* **46**, 781–789 (2007).
171. Herron, J. A. & Maravelias, C. T. Assessment of solar-to-fuels strategies: photocatalysis and electrocatalytic reduction. *Energy Technol.* **4**, 1369–1391 (2016).
172. Xia, Y.-S. et al. Tandem utilization of CO_2 photoreduction products for the carbonylation of aryl iodides. *Nat. Commun.* **13**, 2964 (2022).
173. Song, L. et al. Visible-light photocatalytic di- and hydro-carboxylation of unactivated alkenes with CO_2. *Nat. Catal.* **5**, 832–838 (2022).
174. Ulmer, U. et al. Fundamentals and applications of photocatalytic CO_2 methanation. *Nat. Commun.* **10**, 3169 (2019).
175. Tavasoli, A. V., Preston, M. & Ozin, G. Photocatalytic dry reforming: what is it good for? *Energy Environ. Sci.* **14**, 3098–3109 (2021).
176. von der Assen, N., Voll, P., Peters, M. & Bardow, A. Life cycle assessment of CO_2 capture and utilization: a tutorial review. *Chem. Soc. Rev.* **43**, 7982–7994 (2014).
177. Trudewind, C. A., Schreiber, A. & Haumann, D. Photocatalytic methanol and methane production using captured CO_2 from coal-fired power plants. Part I — a life cycle assessment. *J. Clean. Prod.* **70**, 27–37 (2014).
178. Lewis, N. S. Developing a scalable artificial photosynthesis technology through nanomaterials by design. *Nat. Nanotechnol.* **11**, 1010–1019 (2016).
179. Faunce, T. et al. Artificial photosynthesis as a frontier technology for energy sustainability. *Energy Environ. Sci.* **6**, 1074–1076 (2013).
180. Li, M., Sun, Z. & Hu, Y. H. Thermo-photo coupled catalytic CO_2 reforming of methane: a review. *Chem. Eng. J.* **428**, 131222 (2022).
181. Shoji, S. et al. Photocatalytic uphill conversion of natural gas beyond the limitation of thermal reaction systems. *Nat. Catal.* **3**, 148–153 (2020).
182. Ye, R.-P. et al. CO_2 hydrogenation to high-value products via heterogeneous catalysis. *Nat. Commun.* **10**, 5698 (2019).
183. Wu, X. et al. Photocatalytic CO_2 conversion of $M_{0.33}WO_3$ directly from the air with high selectivity: insight into full spectrum-induced reaction mechanism. *J. Am. Chem. Soc.* **141**, 5267–5274 (2019).
184. Wang, L. et al. Bismuth vacancy-induced efficient CO_2 photoreduction in BiOCl directly from natural air: a progressive step toward photosynthesis in nature. *Nano Lett.* **21**, 10260–10266 (2021).
This work uses natural air as CO_2 feedstock, which is an important practice towards applications.
185. Schäppi, R. et al. Drop-in fuels from sunlight and air. *Nature* **601**, 63–68 (2022).
186. Li, Z. et al. Engineered disorder in CO_2 photocatalysis. *Nat. Commun.* **13**, 7205 (2022).
187. Zhang, Y. et al. Photocatalytic CO_2 reduction: identification and elimination of false-positive results. *ACS Energy Lett.* **7**, 1611–1617 (2022).
188. Kant, P., Liang, S., Rubin, M., Ozin, G. A. & Dittmeyer, R. Low-cost photoreactors for highly photon/energy-efficient solar-driven synthesis. *Joule* **7**, 1347–1362 (2023).
189. Zhao, Y. et al. Defect-rich ultrathin ZnAl-layered double hydroxide nanosheets for efficient photoreduction of CO_2 to CO with water. *Adv. Mater.* **27**, 7824–7831 (2015).
190. Yan, T. et al. Bismuth atom tailoring of indium oxide surface frustrated Lewis pairs boosts heterogeneous CO_2 photocatalytic hydrogenation. *Nat. Commun.* **11**, 6095 (2020).
191. Cai, M. et al. Greenhouse-inspired supra-photothermal CO_2 catalysis. *Nat. Energy* **6**, 807–814 (2021).
This work develops a core–shell structured photocatalyst with strong photo-thermal effect for CO_2 hydrogenation.
192. Xie, S. et al. Photocatalytic reduction of CO_2 with H_2O: significant enhancement of the activity of Pt–TiO_2 in CH_4 formation by addition of MgO. *Chem. Commun.* **49**, 2451–2453 (2013).
193. Wang, T. et al. In situ synthesis of ordered mesoporous co-doped TiO_2 and its enhanced photocatalytic activity and selectivity for the reduction of CO_2. *J. Mater. Chem. A* **3**, 9491–9501 (2015).
194. Xing, M. et al. Modulation of the reduction potential of TiO_{2-x} by fluorination for efficient and selective CH_4 generation from CO_2 photoreduction. *Nano Lett.* **18**, 3384–3390 (2018).
195. Niu, P., Yang, Y., Yu, J. C., Liu, G. & Cheng, H.-M. Switching the selectivity of the photoreduction reaction of carbon dioxide by controlling the band structure of a g-C_3N_4 photocatalyst. *Chem. Commun.* **50**, 10837–10840 (2014).
196. Fu, J., Jiang, K., Qiu, X., Yu, J. & Liu, M. Product selectivity of photocatalytic CO_2 reduction reactions. *Mater. Today* **32**, 222–243 (2020).
197. Bai, S. et al. Two-dimensional g-C_3N_4: an ideal platform for examining facet selectivity of metal co-catalysts in photocatalysis. *Chem. Commun.* **50**, 6094–6097 (2014).
198. Zhang, H. et al. Surface-plasmon-enhanced photodriven CO_2 reduction catalyzed by metal–organic-framework-derived iron nanoparticles encapsulated by ultrathin carbon layers. *Adv. Mater.* **28**, 3703–3710 (2016).
199. Singh, A. K., Montoya, J. H., Gregoire, J. M. & Persson, K. A. Robust and synthesizable photocatalysts for CO_2 reduction: a data-driven materials discovery. *Nat. Commun.* **10**, 443 (2019).
To our knowledge, this is the first report on applying first-principles computation to screen the robust and synthesizable photocatalysts for CO_2 reduction.
200. Stach, E. et al. Autonomous experimentation systems for materials development: a community perspective. *Matter* **4**, 2702–2726 (2021).
201. Wang, A., Bozal-Ginesta, C., Hari Kumar, S. G., Aspuru-Guzik, A. & Ozin, G. A. Designing materials acceleration platforms for heterogeneous CO_2 photo(thermal)catalysis. *Matter* **6**, 1334–1347 (2023).
202. Rao, H., Lim, C.-H., Bonin, J., Miyake, G. M. & Robert, M. Visible-light-driven conversion of CO_2 to CH_4 with an organic sensitizer and an iron porphyrin catalyst. *J. Am. Chem. Soc.* **140**, 17830–17834 (2018).
203. Andrei, V. et al. Long-term solar water and CO_2 splitting with photoelectrochemical BiOI–$BiVO_4$ tandems. *Nat. Mater.* **21**, 864–868 (2022).
204. Bhattacharjee, S. et al. Photoelectrochemical CO_2-to-fuel conversion with simultaneous plastic reforming. *Nat. Synth.* **2**, 182–192 (2023).
205. Pati, P. B. et al. Photocathode functionalized with a molecular cobalt catalyst for selective carbon dioxide reduction in water. *Nat. Commun.* **11**, 3499 (2020).
206. Wang, S. et al. Grave-to-cradle upcycling of Ni from electroplating wastewater to photothermal CO_2 catalysis. *Nat. Commun.* **13**, 5305 (2022).
207. Xu, Y.-F. et al. High-performance light-driven heterogeneous CO_2 catalysis with near-unity selectivity on metal phosphides. *Nat. Commun.* **11**, 5149 (2020).
208. Yu, S., Wilson, A. J., Heo, J. & Jain, P. K. Plasmonic control of multi-electron transfer and C–C coupling in visible-light-driven CO_2 reduction on Au nanoparticles. *Nano Lett.* **18**, 2189–2194 (2018).
209. Sun, Z., Ma, T., Tao, H., Fan, Q. & Han, B. Fundamentals and challenges of electrochemical CO_2 reduction using two-dimensional materials. *Chem* **3**, 560–587 (2017).
210. Fang, S. & Hu, Y. H. Temperature, pressure, and adsorption-dependent redox potentials: I. Processes of CO_2 reduction to value-added compounds. *Energy Sci. Eng.* **10**, 4520–4543 (2022).
211. Xu, F. et al. Unique S-scheme heterojunctions in self-assembled TiO_2/$CsPbBr_3$ hybrids for CO_2 photoreduction. *Nat. Commun.* **11**, 4613 (2020).
212. Bae, K.-L., Kim, J., Lim, C. K., Nam, K. M. & Song, H. Colloidal zinc oxide-copper(I) oxide nanocatalysts for selective aqueous photocatalytic carbon dioxide conversion into methane. *Nat. Commun.* **8**, 1156 (2017).
213. Liu, Y. et al. Phase-enabled metal–organic framework homojunction for highly selective CO_2 photoreduction. *Nat. Commun.* **12**, 1231 (2021).
214. Chen, X. et al. Bromo- and iodo-bridged building units in metal–organic frameworks for enhanced carrier transport and CO_2 photoreduction by water vapor. *Nat. Commun.* **13**, 4592 (2022).

Acknowledgements

Y.H.H. and S.F. acknowledge the support from the National Science Foundation (CMMI-1661699). M. Rahaman acknowledges the support from the European Commission with a Horizon 2020 Marie Skłodowska-Curie Individual European Fellowship (SolarFUEL, GAN 839763). E.R. acknowledges the support for a European Research Council (ERC) Consolidator Grant (MatEnSAP, no. 682833). M. Robert acknowledges the Institut Universitaire de France (IUF) for partial financial support.

Author contributions

Introduction (S.F., J.B., E.R., M. Robert, G.A.O. and Y.H.H.); Experimentation (S.F., M. Rahaman, J.B., E.R., M. Robert, G.A.O. and Y.H.H.); Results (S.F., M. Rahaman, E.R., M. Robert, G.A.O. and Y.H.H.); Applications (S.F., E.R., M. Robert, G.A.O. and Y.H.H.); Reproducibility and data deposition (S.F., J.B., E.R., M. Robert, G.A.O. and Y.H.H.); Limitations and optimizations (S.F., E.R., M. Robert, G.A.O. and Y.H.H.); Outlook (S.F., E.R., M. Robert, G.A.O. and Y.H.H.); overview of the Primer (S.F., M. Rahaman, J.B., E.R., M. Robert, G.A.O. and Y.H.H.).

Competing interests

The authors declare no competing interests.

Additional information

Peer review information *Nature Reviews Methods Primers* thanks Vivek Polshettiwar and the other, anonymous, reviewer(s) for their contribution to the peer review of this work.

Related links

ChemAnalyst: http://www.chemanalyst.com
US Energy Information Administration: http://www.eia.gov/